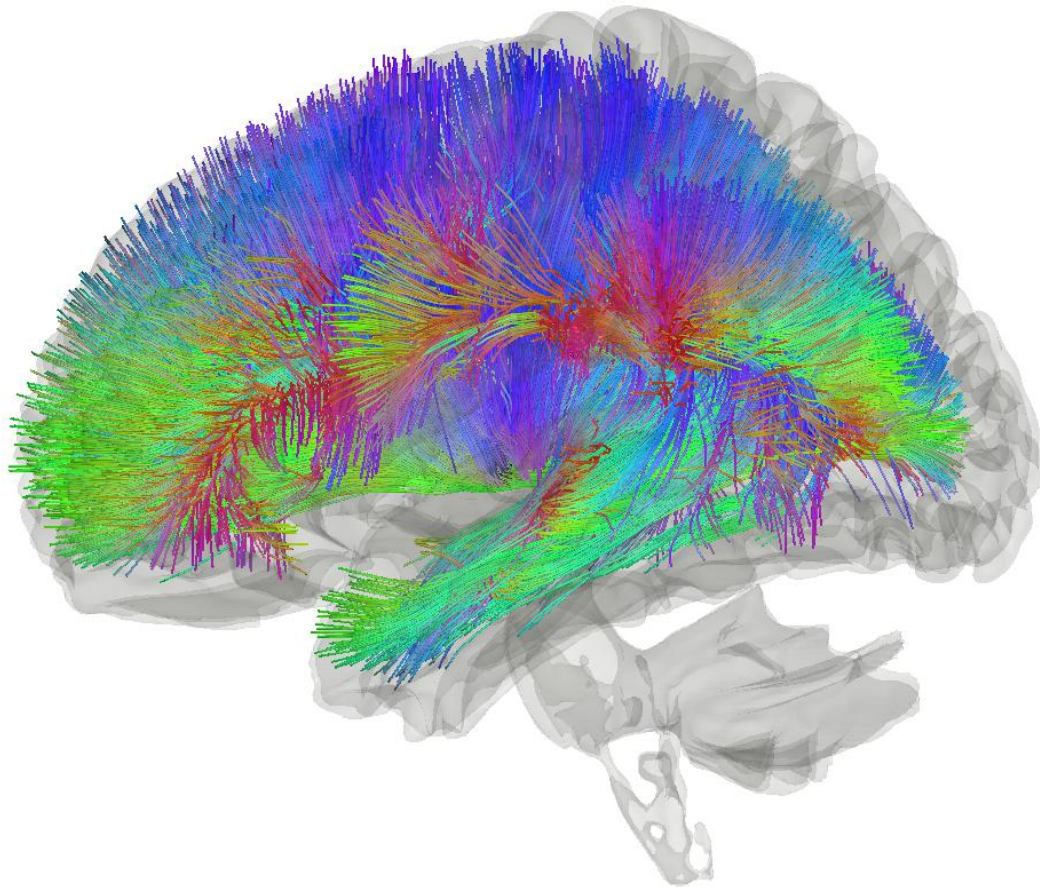




CHALMERS
UNIVERSITY OF TECHNOLOGY



Biophysically Realistic Thalamocortical Neural Mass Model

Model evaluation and simulation of sleep stages

Joint master's thesis in Engineering Mathematics and Computational Science & Complex Adaptive Systems

MATTIAS JOHNSON & ANTON ERIKSSON

DEPARTMENT OF MATHEMATICAL SCIENCES

CHALMERS UNIVERSITY OF TECHNOLOGY
Gothenburg, Sweden 2022
www.chalmers.se

MASTER'S THESIS 2022

Biophysically Realistic Thalamocortical Neural Mass Model

Model evaluation and simulation of sleep stages

MATTIAS JOHNSON & ANTON ERIKSSON



CHALMERS
UNIVERSITY OF TECHNOLOGY

Department of Mathematical Sciences
CHALMERS UNIVERSITY OF TECHNOLOGY
Gothenburg, Sweden 2022

Biophysically Realistic Thalamocortical Neural Mass Model
Model evaluation and simulation of sleep stages
MATTIAS JOHNSON & ANTON ERIKSSON

© MATTIAS JOHNSON & ANTON ERIKSSON, 2022.

Supervisor: Prof. Dr. Klaus Obermayer, Neural Information Processing Group, TU
Berlin
Examiner: Gerlee, Philip

Master's Thesis 2022
Department of Mathematical Sciences Chalmers University of Technology
SE-412 96 Gothenburg
Telephone +46 31 772 1000

Cover: Visualization of brain tractography [2].
Typeset in L^AT_EX
Printed by Chalmers Reproservice
Gothenburg, Sweden 2022

Biophysically Realistic Thalamocortical Neural Mass Model
Model evaluation and simulation of sleep stages
MATTIAS JOHNSON & ANTON ERIKSSON
Department of Mathematical Sciences
Chalmers University of Technology

Abstract

For analysing a complex system such as the brain mathematical modeling and simulation are increasingly important tools. This analysis can be performed on scales ranging from the neuron to so called neural mass models simulating whole brain regions. By using the computational framework for whole-brain modeling called Neurolib we have combined its cortical and thalamic models into a single model which we call the thalamocortical model. This model was 12 times faster than the previous Neurolib implementation. Neurolib provides structural data which made it possible to create models with biologically informed connectivity. With this data we created a two-node model (a single thalamic and cortical node) and an 80+1-node model (80 cortical nodes). Through various simulations and analysing both models we found satisfactory points in the parameter space which gave rise to qualitative behaviour associated with both a sleeping brain and an awake brain, the behaviours in question include phenomena such as slow oscillations and sleep spindles.

Keywords: Computational neuroscience, neural mass models, sleeping stages, thalamocortical model

Acknowledgements

We want thank Prof. Dr. Klaus Obermayer and everybody at The Neural Information Processing Group at Technische Universität Berlin for the opportunity to do our master's thesis with you. Special thanks to Nikola Jaycay, Caglar Cakan and Cristoph Metzner for supervising and helping us throughout the project. We also want to thank Philip Gerlee, our examiner at Chalmers University of Technology.

Contents

List of Figures	xi
1 Introduction	3
1.1 Background	3
1.2 Related work	4
1.2.1 ALN	4
1.2.2 80-node model	4
1.2.3 2-node model	4
1.2.4 Parameters	4
1.3 Limitations	5
2 Theory	7
2.1 The biological brain	7
2.1.1 Neurons & synapses	7
2.1.2 Cerebral cortex	8
2.1.3 Thalamus	9
2.1.4 Neuroimaging	9
2.1.4.1 EEG	9
2.2 The sleeping brain	10
2.3 The simulated brain	11
2.3.1 Neuron models	11
2.3.1.1 Leaky integrator / passive membrane	11
2.3.1.2 Leaky integrate-and-fire model (LIF)	12
2.3.1.3 Exponential integrate-and-fire model (EIF)	12
2.3.1.4 Adaptive Exponential integrate-and-fire model (AdEx)	13
2.3.1.5 Hodgkin-Huxley Model	13
2.3.2 Whole-brain models	14
2.3.2.1 Mean-field models	14
2.3.3 Neurolib	15
3 Methods	17
3.1 Cortical model	17
3.1.1 Noise input μ_{α}^{ou} in cortical model	18
3.2 Thalamic model	18
3.3 Thalamocortical model	20
3.3.1 Connection thalamus \rightarrow cortex	20

3.3.2	Connection cortex \rightarrow thalamus	20
3.4	Node connections in a 80+1-node whole-brain model	20
3.5	Signal analysis	21
3.5.1	EEG Dataset	21
3.5.2	Power spectrums	21
3.5.3	Summary statistics	21
3.5.4	Spindles	21
3.6	Parameter search	22
4	Results	23
4.1	Thalamocortical implementation	23
4.2	2-node model	24
4.2.1	Sleeping state	24
4.2.2	Awake state	25
4.2.2.1	Exploration of individual parameters	25
4.2.2.2	Exploration of two parameters at a time	27
4.3	81-node model	32
4.3.1	Sleeping state	32
4.3.2	Awake state	36
5	Discussion	39
5.1	2-node model	39
5.1.1	Sleeping state	39
5.1.2	Awake state	39
5.1.2.1	Exploration of individual parameters	39
5.1.2.2	Exploration of two parameters at a time	39
5.2	81-node model	40
5.2.1	Sleeping state	40
5.2.2	Awake state	41
6	Conclusion	43
	Bibliography	45
A	Parameters	I
A.1	Model Parameters	I
A.1.1	Parameters from Cakan et al. [11]	III

List of Figures

2.1	Figure of the basic components of a neuron (from [3]).	8
2.2	Subject ready for EEG recording (from [22]).	9
2.3	Sample EEG from human (from [14]).	10
2.4	Electronics representation of a leaky integrator.	12
2.5	Electronics representation of a Hodgkin-Huxley model.	14
4.1	Runtimes of the existing thalamus-cortex implementation in Neurolib Multimodel compared to the implemented thalamocortical model. The thalamocortical model was an order of magnitude faster taking only 8.3% of the time the multimodel took with the runtime mean and standard deviations being 252 ± 0.688 ms compared to 3040 ± 11.4 ms. The runtime statistics were calculated after 100 runs with the models running a 10000 ms simulation with the timestep of 0.1 ms.	23
4.2	The figure shows a 20 second time excerpt of the firing rate of the excitatory population in the cortical node. The simulation was run with one cortical and one thalamic node with parameters from tables A.1, A.2 and A.3 in Appendix A.1.	24
4.3	The figure shows a 20 second time excerpt of the firing rate of the thalamocortical relay population in the thalamic node. The simulation was run with one cortical and one thalamic node with parameters from tables A.1, A.2 and A.3 in Appendix A.1.	24
4.4	The figure shows the power spectrum of the firing rate in the excitatory population from a 120 second simulation. The simulation was run with one cortical and one thalamic node with parameters from tables A.1, A.2 and A.3 in Appendix A.1.	25
4.5	The figure shows the frequency of the most prominent peak in a power spectrum between 7.5 Hz and 15 Hz of the firing rate in the excitatory population in the cortical node from a 120 second simulation for varying values of w_i^r . The simulations were run with one cortical and one thalamic node with parameters from tables A.1, A.2 and A.3 in Appendix A.1 as starting point. Note that the frequency of the peak varies substantially over the range.	26

- 4.6 The figure shows the frequency of the most prominent peak in a power spectrum between 7.5 Hz and 15 Hz of the firing rate in the excitatory population in the cortical node from a 120 second simulation for varying values of w_i^t . The simulations were run with one cortical and one thalamic node with parameters from tables A.1, A.2 and A.3 in Appendix A.1 as starting point. Note that the frequency of the peak varies substantially over the range. 26
- 4.7 The figure shows a 20 second time excerpt of the firing rate of the thalamocortical relay population in the thalamic node. The simulation was run with one cortical and one thalamic node with $w_i^r = 0.5$. The rest of the parameters are from tables A.1, A.2 and A.3 in Appendix A.1. 27
- 4.8 The figure shows the power spectrum of the firing rate in the excitatory population in the cortical node from a 120 second simulation. The simulation was run with one cortical and one thalamic node with $w_i^r = 0.5$. The rest of the parameters are from tables A.1, A.2 and A.3 in Appendix A.1. Note the peak at about 10 Hz. 27
- 4.9 The figure shows the difference between the maximum and the minimum value of the firing rate of the thalamocortical relay population in the thalamic node from a 120 second simulation, for varying values of w_i^r and w_i^t . The rest of the parameters are from tables A.1, A.2 and A.3 in Appendix A.1. $w_i^t = 1.27, w_i^r = 0.5$ is marked with a green star. 28
- 4.10 The figure shows the average spindle amplitude of the firing rate of the thalamocortical relay population in the thalamic node from a 120 second simulation, for varying values of w_i^r and w_i^t . The rest of the parameters are from tables A.1, A.2 and A.3 in Appendix A.1. $w_i^t = 1.27, w_i^r = 0.5$ is marked with a green star. 29
- 4.11 The figure shows the prominence of the most prominent peak in the range 8Hz to 12Hz in a power spectrum of the firing rate in the excitatory population in the cortical node from a 120 second simulation, for varying values of w_i^r and w_i^t . The rest of the parameters are from tables A.1, A.2 and A.3 in Appendix A.1. $w_i^t = 1.27, w_i^r = 0.5$ is marked with a green star. 30
- 4.12 The figure shows a 20 second time excerpt of the firing rate of the excitatory population in the cortical node. The simulation was run with one cortical and one thalamic node with $w_i^t = 1.27, w_i^r = 0.5$. The rest of the parameters are from tables A.1, A.2 and A.3 in Appendix A.1. 31
- 4.13 The figure shows a 20 second time excerpt of the firing rate of the thalamocortical relay population in the thalamic node. The simulation was run with one cortical and one thalamic node with $w_i^t = 1.27, w_i^r = 0.5$. The rest of the parameters are from tables A.1, A.2 and A.3 in Appendix A.1. 31

4.14	The figure shows the power spectrum of the firing rate in the excitatory population in the cortical node from a 120 second simulation. The simulation was run with one cortical and one thalamic node with $w_i^t = 1.27, w_i^r = 0.5$. The rest of the parameters are from tables A.1, A.2 and A.3 in Appendix A.1. Note the peak at about 10 Hz.	31
4.15	The figure shows the spindling frequency of the firing rates of thalamocortical relay population in the thalamic node from a 60 second simulation, for varying values of b and μ_E . Parameters are from Table A.4 in Appendix A.1.1. The other parameters are from tables A.1, A.2 and A.3 in Appendix A.1. $\text{mue_ext_mean} = 2.5, b = 2.3$ is marked with a blue star.	33
4.16	The figure shows the mean value in the range 7.5Hz to 15Hz of the mean power spectrum of the firing rates of the excitatory populations in the cortical nodes from a 60 second simulation, for varying values of b and μ_E . Table A.4 in Appendix A.1.1. The other parameters are from tables A.1, A.2 and A.3 in Appendix A.1. $\text{mue_ext_mean} = 2.5, b = 2.3$ is marked with a blue star.	34
4.17	The figure shows a 20 second time excerpt of the mean of the firing rate of the excitatory population in all 80 cortical nodes. The simulation was run with 80 cortical nodes and one thalamic node with parameters from Table A.4 in Appendix A.1.1. The other parameters are from tables A.1, A.2 and A.3 in Appendix A.1.	35
4.18	The figure shows a 20 second time excerpt of the firing rate of the thalamocortical relay population in the thalamic node. The simulation was run with 80 cortical nodes and one thalamic node with parameters from Table A.4 in Appendix A.1.1. The other parameters are from tables A.1, A.2 and A.3 in Appendix A.1.	35
4.19	The figure shows the mean power spectrum of the firing rate in the excitatory population in all cortical nodes from a 120 second simulation. The simulations were run with 80 cortical nodes and one thalamic node with parameters from Table A.4 in Appendix A.1.1. The other parameters are from tables A.1, A.2 and A.3 in Appendix A.1. Note the peak at about 10 Hz.	36
4.20	The figure shows a 20 second time excerpt of the mean of the firing rate of the excitatory populations in all 80 cortical nodes. The simulation was run with 80 cortical nodes and one thalamic node with $w_i^t = 1.27, w_i^r = 0.5$ and with parameters from Table A.4 in Appendix A.1.1. The other parameters are from tables A.1, A.2 and A.3 in Appendix A.1.	36
4.21	The figure shows a 20 second time excerpt of the firing rate of the thalamocortical relay population in the thalamic node. The simulation was run with 80 cortical nodes and one thalamic node with $w_i^t = 1.27, w_i^r = 0.5$ and with parameters from Table A.4 in Appendix A.1.1. The other parameters are from tables A.1, A.2 and A.3 in Appendix A.1.	37

- 4.22 The figure shows the mean power spectrum of the firing rate in the excitatory populations in all cortical nodes from a 120 second simulation. The simulation was run with 80 cortical nodes and one thalamic node with $w_i^t = 1.27, w_i^r = 0.5$ and with parameters from Table A.4 in Appendix A.1.1. The other parameters are from tables A.1, A.2 and A.3 in Appendix A.1. Note the peak at 10 Hz. 37

1

Introduction

1.1 Background

The objective of this project was to create a model of the brain and have it replicate both a brain in an awake state and a sleeping state. In order to achieve this objective it is of course not feasible to simulate each of the brain’s 86 billion neurons where every neuron then averages 7000 synaptic connections. Instead one can use a neural mass model, that is using a low-dimensional model representation of the activity of large populations of neurons and synapses. In much the same way, instead of simulating every region of the brain one can simulate the regions of interest with added noise approximating the input from the non-included brain regions. In this case the regions of interest — that is the regions showing particular activity in sleep — are the cortex together with the thalamus.

Neurolib is an open-source simulation framework containing several neural mass models implemented in Python including a cortical and a thalamic model. The Neurolib framework also includes a way of running a cortical model connected with a thalamic model, a so called thalamocortical model. This can be achieved by using an included framework called multimodel which makes it easy to combine different neural models. The problem is that the ease of use comes with some performance drawbacks, especially noticeable when one wants to not only simulate a single cortical unit but 80 separate cortical nodes representing different brain areas. This motivates a faster implementation of the thalamocortical model.

The two central questions which we answer in this report are “*How well did the implemented thalamocortical model replicate the sleeping and awake state of real biological brains?*” and “*How exactly is the thalamocortical neural model constructed?*”. Corollary questions demanding answers are: what are the central characteristics of sleeping and awake brains relevant for our simulations, what type of empirical data is used, what is the motivation behind using a low-dimensional representation of the brain?

1.2 Related work

This project is based on the results and methodologies of four papers, three of which establish the neural models used and one of which gives the relevant parameters to examine in order to model sleeping and awake brain states.

1.2.1 ALN

In ‘Biophysically grounded mean-field models of neural populations under electrical stimulation’ by Cakan and Obermayer [13] they set about the problem that large spiking neural networks are hard to simulate and analyze when investigating the effects of electrical stimulation. They investigated if a mean-field model of adaptive exponential integrate-and-fire (AdEx) neurons could be a solution to this problem. In the paper they present results showing that the created model has some desired qualities and that it gives good predictions of the behaviour of a spiking network of individual AdEx neurons. The model implemented is the model that we use in this project to simulate cortical neural populations.

1.2.2 80-node model

In ‘Spatiotemporal patterns of adaptation-induced slow oscillations in a whole-brain model of slow-wave sleep’ [11] Cakan et al. – instead of a model consisting of a single ALN node – evaluate a model consisting of 80 connected ALN nodes. They use evolutionary optimization to fit the model to human EEG and fMRI data. It is shown that the model can produce realistic local and global slow oscillations (SOs). They conclude that the traveling global waves are caused by the connectome, i.e. the different connection strengths between the nodes. The 81-node model used in this project is equivalent to the 80 node model used by Cakan et al. if the thalamic node is removed.

1.2.3 2-node model

Jaycay et al. are investigating a thalamocortical model in the paper ‘Cross-Frequency Slow Oscillation–Spindle Coupling in a Biophysically Realistic Thalamocortical Neural Mass Model’ [20]. They couple a thalamic model with an ALN node to investigate SOs and sleep spindles. By varying different parameters in the model they find that the model can produce experimentally observed interactions between SOs and spindles. The equations defining the two-node model in our project are the same as in this paper by Jaycay et al.

1.2.4 Parameters

Krishnan et al. investigates the effect of neuromodulators on a thalamocortical model in the paper ‘Cellular and neurochemical basis of sleep stages in the thalam-

ocortical network' [23]. By exploring different parameters they find a set of parameters that when varied can generate characteristic brain EEG rhythms for different states (different sleeping states and awake state). The parameters investigated in our project are based on the parameters found by Krishnan et al.

1.3 Limitations

For simulating such a complex system as the brain there are a set of limitations one has to adhere to for it to be feasible. Individual neurons are not simulated but instead models which approximate whole populations of neurons through mean-field theory are used. All of the constituent parts of the brain are not taken into account, instead only the cortex and the thalamus are included in simulations since a sleeping brain's activity mainly stems from these two. In this model the input coming from the rest of the brain to the cortex and thalamus is approximated as noise.

For simulating a sleeping state we did not include all the sleeping stages but instead only the N2/N3 sleep stages grouped together as one and we did not include all the characteristics of those stages either but had a goal to find a state containing sleep spindles and slow oscillations. For the awake state we limited our search for characteristics to be an alpha peak and no spindling. Finally the model parameters examined for state changes are limited to the parameters examined by Krishnan et al [23].

2

Theory

2.1 The biological brain

The human brain is a highly complex system consisting of heterogeneous interacting parts on multiple scales. This includes different types of neurons all the way up to different regions of the brain specialising at certain tasks. In the following sections we present some fundamental requisitory knowledge about relevant regions and mechanisms.

2.1.1 Neurons & synapses

The basic building block of all parts of the brain is the neuron. In this section the neuron will be described on a level of abstraction sufficient for understanding the mechanisms relevant to this project.

The functions that are important are the ability to receive signals from other neurons, process these signals non-linearly and emit signals to other neurons [17]. The principal parts of neurons are the dendrites, the soma and the axon (see Figure 2.1). The soma is the cell's body containing the machinery needed for the cell to survive including genetic material and mitochondria, dendrites receive signals and axons are the exit terminal connecting to the dendrites of other neurons.

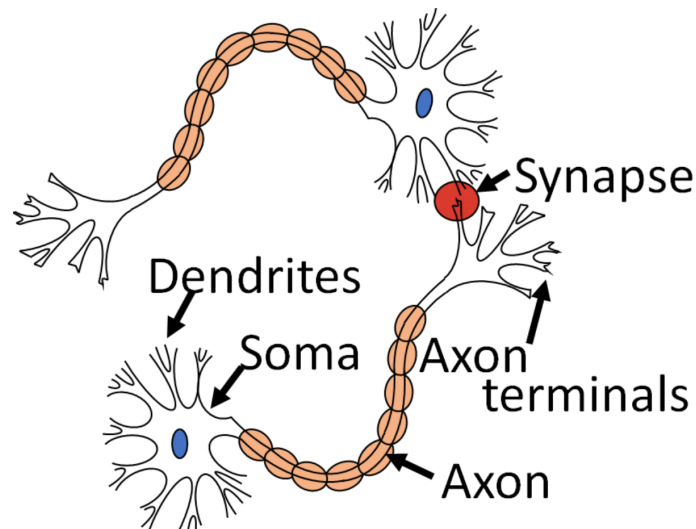


Figure 2.1: Figure of the basic components of a neuron (from [3]).

The output of a neuron is an electrical signal called a spike or an action potential. When a neuron receives enough input it will generate a spike. As mentioned above however it is not a linear function. It does not only depend on the amplitude of the membrane potential and the exact behaviours are not completely understood. And it is not the spike in itself that carries the information, but the frequency and timing of the spikes.

The spike travels through the axon to other neurons. The site where neurons connect is called the synapse. The most common form of synapses are chemical synapses. They transmit the signal by releasing neurotransmitters that then generates an electrical signal in the postsynaptic cell. In the brain there are also so called neuromodulators present which regulate the behaviour of populations of neurons, common examples of neuromodulators include acetylcholine, histamine, GABA and serotonin.

2.1.2 Cerebral cortex

The cerebral cortex is the most highly developed part of the human brain and is responsible for higher-level cognitive functions such as perceiving, thinking and understanding language. It is an on average 2.5 mm thin layer of grey matter covering all of the cerebrum which is the largest and uppermost portion of the brain made up of the two cerebral hemispheres. The cerebral cortex still makes up around two thirds of the brains total mass (which in total weighs about 1336 grams in males and 1198 grams in females)[18, 21]. It is a highly folded sheet with its bulges being called gyri and fissures called sulci. The folding adds to the surface area which adds more gray matter thereby increases the information it can process. The folding creates separate brain regions and it is the basis for the division in the AAL2 atlas which divides the cerebral cortex into 80 separate nodes and is the data used in the brain simulation framework Neurolib (see Section 2.3.3) as well as in our thesis for simulation of the cerebral cortex [29].

2.1.3 Thalamus

As with most parts of the brain the thalamus has multiple functions such as roles in motor activity, emotion and memory. It is however classically known for relaying sensory impulses from various parts of the body to the cerebral cortex. A sensory impulse would travel from the body's surface to the thalamus where it is received as a sensation to be passed to the cerebral cortex for interpretation as temperature, touch or pain. It is crucial for perception as all sensory input is relayed by it with the sole exception of smell. The thalamus is located near the center of the brain with connections out to the cerebral cortex in all directions [4, 1].

2.1.4 Neuroimaging

Neuroimaging is the process of recording different aspects of the brain. It provides quantitative data which links computational neuroscience to the real world and is therefore necessary to the field. There exist many different technologies that differ in spatial and temporal resolution. The data relevant to this study is Electroencephalography (EEG).

2.1.4.1 EEG

Electroencephalography (EEG) measures voltage variations resulting from ionic current within the brain's neurons. This is done by placing electrodes on the scalp and these types of measurements of electrical activity on tissue are called electrograms (see Figure 2.2 and Figure 2.3) [8]. The simplicity of the technique allows for a very high temporal resolution while it has a relatively low spatial resolution, and it can only measure the activity on the surface layer of the brain. EEG recordings are typically analysed by calculating what is called the power spectrum of the signal or signals (see Section 3.5.2 for description).

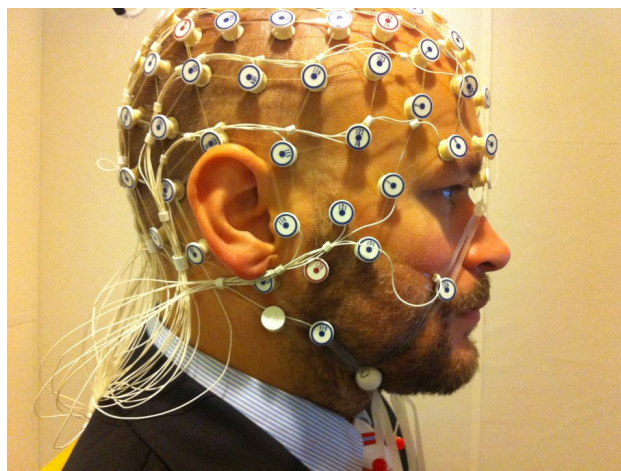


Figure 2.2: Subject ready for EEG recording (from [22]).

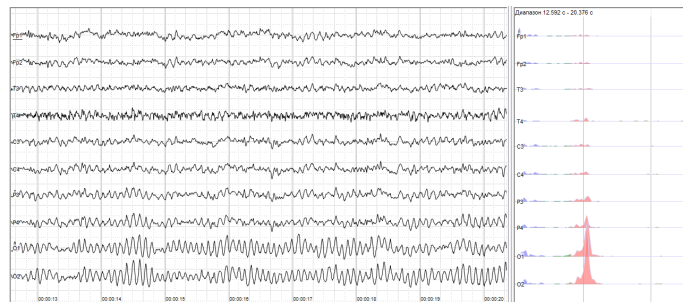


Figure 2.3: Sample EEG from human (from [14]).

2.2 The sleeping brain

The sleeping brain's activity is characterized by different types of oscillations in its thalamocortical and hippocampal networks. The oscillations include, among others, so called slow waves, sleep spindles, alpha and theta waves (see below for definitions). These oscillations in the brain's activity are so central to sleep that they are the basis for the classification of sleep into its different sleep stages. The latest revision to the system of sleep stages was 2007 and comes from the America Academy of Sleep Medicine which devised a system consisting REM sleep and three stages of Non-REM sleep (N1-N3) [6, 27].

The first and shortest sleep stage is the N1 stage. In the N1 sleep the body transitions from wakefulness to sleep. The stage lasts several minutes and is marked by slowing down of the heartbeat, breathing and eye movement and relaxation of the muscles [1]. The brain transition from alpha waves (8-12 Hz) to theta waves (4-8 Hz).

Following the N1 Stage is the N2. Theta waves are observed and alpha waves are diminished or disappear. This sleep stage makes up around 45-55 % of sleep. In this stage there is also another type of oscillation called sleep spindles wherein the thalamus and cortex together give rise to alternations between high and low activity states called UP and DOWN states. These spindles can range in frequency from 7 to 15 Hz.

In the third non-REM sleep stage, also called deep sleep or slow-wave sleep there are delta waves ranging from 0.5-2 Hz. The sleeper is less responsive to the environment in this stage.

In rapid-eye-movement sleep (REM sleep), as the name implies, the eyes move rapidly (all the muscles under conscious control are paralysed except for the eye muscles). It is in this stage that the sleeper may have vivid dream.

Sleep typically consists of 4 to 5 sleep cycles, as mentioned N1 is the stage in which the subject is falling asleep and thereafter the progression of sleep stages in each cycle is the following:

$$N2 \rightarrow N3 \rightarrow N2 \rightarrow \text{REM}.$$

2.3 The simulated brain

Mathematical models and computer simulations are key tools for reaching a better level of understanding of such a complex system as the brain. Examples of this include studying the differential effects of neuromodulators [15], studying the role of transmission delays between brain areas [10], explaining features of electroencephalogram [16] and explaining the propagation of brain waves [28]. There exists a wide variety of brain models on different scales ranging from the singular neuron to the macroscopic scale called neural mass models which approximate large populations of neurons. The Python framework for brain simulations Neurolib (see Section 2.3.3) works on the macroscopic scale of brain modelling. The different brain regions are coupled through long-range axonal connections. Computationally these regions will also be referred to as nodes.

2.3.1 Neuron models

Both of the thalamic and cortical brain models used in this report have their foundation in simpler neuron-level models. This section is dedicated to describing those neuron models starting from the simple Leaky integrator up until the Hodgkin-Huxley and Adaptive Exponential integrate-and-fire model which are the foundation for the models used in this report.

2.3.1.1 Leaky integrator / passive membrane

The *Leaky integrator* can be modeled through electronics laws [17] (see Figure 2.4).

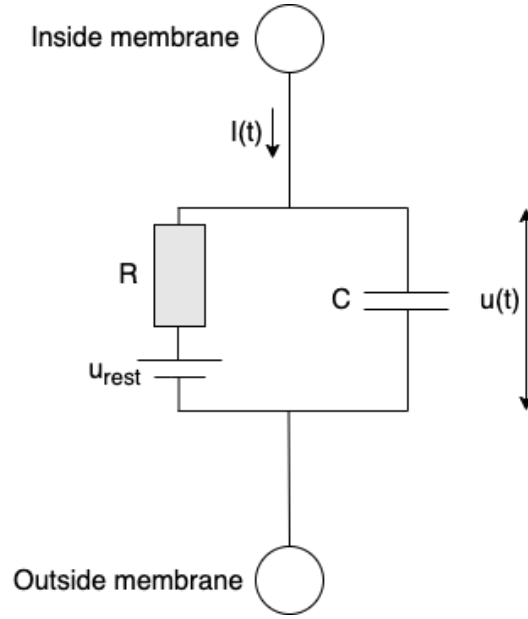


Figure 2.4: Electronics representation of a leaky integrator.

We call the potential over the cell membrane of a neuron its *membrane potential* $u(t)$. When there is no external input to the neuron the potential will be at its *resting potential* u_{rest} which can be modeled with a battery. When a current $I(t)$ is injected to the neuron the membrane potential will deviate from its resting potential and the membrane acts as a capacitor C which is charged. The membrane is not a perfect insulator and the leak can be modeled by a resistance R . We can split the current into the current passing the resistor $I_R(t) = u_R(t)/R = (u(t) - u_{rest})/R$ and the current that charges/discharges the capacitor $I_C(t) = dq/dt = Cdu/dt$. This results in

$$I(t) = I_R(t) + I_C(t) = \frac{u(t) - u_{rest}}{R} + C \frac{du}{dt} \quad (2.1)$$

With the *membrane time constant* $\tau = RC$ we get the standard form of the leaky integrator (or the *equation of a passive membrane*):

$$\tau \frac{du}{dt} = -[u(t) - u_{rest}] + RI(t). \quad (2.2)$$

2.3.1.2 Leaky integrate-and-fire model (LIF)

The LIF is just a leaky integrator in which an action potential is generated when the voltage $u(t)$ goes above a certain threshold u_T [25, 5]. Then the potential is reset to a subthreshold value u_r . This is what ‘fire’ in the name of the model refers to.

2.3.1.3 Exponential integrate-and-fire model (EIF)

In the EIF an exponential term is added:

$$\tau \frac{du}{dt} = -[u(t) - u_{rest}] + \underbrace{\Delta_T \exp\left(\frac{u(t) - \vartheta_{rh}}{\Delta_T}\right)}_{\text{Depolarizing non-linearity}} + RI(t) \quad (2.3)$$

where Δ_T is the sharpness of action potential initiation and ϑ_{rh} is the *intrinsic membrane potential threshold*. Just like in the normal integrate-and-fire model there is also a numerical threshold u_T at which the potential is reset to u_r . However the value of u_T does not matter if it is sufficiently high since the potential approaches infinity very fast.

2.3.1.4 Adaptive Exponential integrate-and-fire model (AdEx)

In the AdEx an adaptation variable is added [9]:

$$\tau \frac{du}{dt} = -[u(t) - u_{rest}] + \Delta_T \exp\left(\frac{u(t) - u_T}{\Delta_T}\right) + RI(t) \underbrace{-Rw}_{\text{Adaptation}} \quad (2.4)$$

$$\tau \frac{dw(t)}{dt} = -a[u(t) - u_{rest}] - w + b\tau\delta(t - t^f) \quad (2.5)$$

where w is the adaptation current and a and b are the coupling parameters. t^f is the firing time and the δ -function increases the adaptation current by b when it fires. The AdEx model is relatively simple given the amount of firing patters it can generate. For example initial bursting which is when a neuron with a constant input current fires more rapidly in the beginning but then starts firing with a lower frequency. In a biophysical neuron adaptation current can be interpreted as certain ions entering the membrane more rapidly during a spike and therefore affects the ion currents after the spike.

2.3.1.5 Hodgkin-Huxley Model

The Hodgkin-Huxley model is similar to the leaky integrator but contains multiple resistor-potential pairs (with the difference that some resistances can be opened or closed depending on voltage) and the equation can be derived in the same way [19]. See Figure 2.5 for the electronics representation where the arrows over the resistors represent that they can be opened or closed. The original Hodgkin-Huxley model takes into account sodium and potassium ion currents plus another unspecified ion current:

$$I(t) = C \frac{du}{dt} + g_K(u - V_K) + g_{Na}(u - V_{Na}) + g_l(u - V_l) \quad (2.6)$$

where g_k , g_{Na} and g_l are the conductances. V_k , V_{Na} and V_l are the reversal potential.

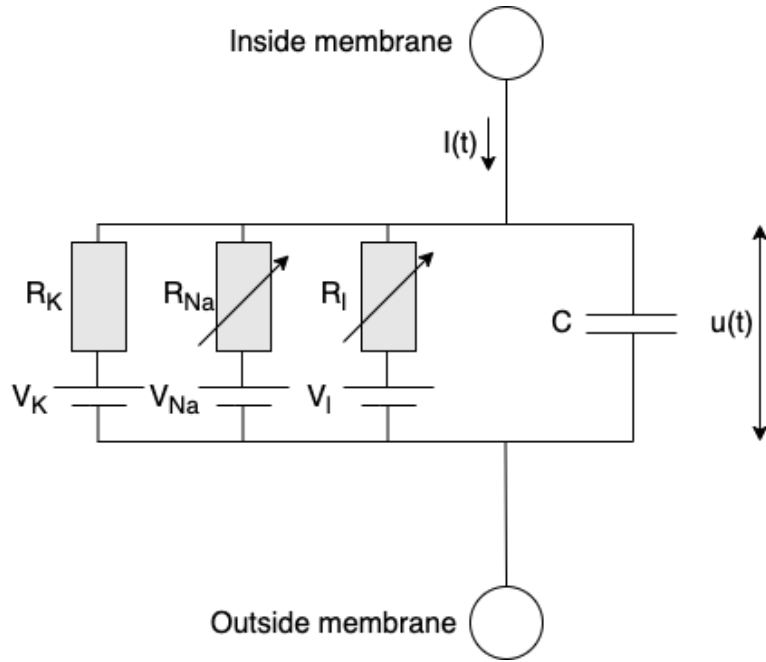


Figure 2.5: Electronics representation of a Hodgkin-Huxley model.

2.3.2 Whole-brain models

A whole-brain model is a model consisting of coupled brain regions. The strength of the coupling between the regions are based on empirical data of the brain usually obtained from diffusion tensor imaging (DTI) which works by measuring the diffusion of water molecules in the brain and is based on the fact that diffusion tends to happen along the direction of axons.

2.3.2.1 Mean-field models

Mean-field theory comes from statistical mechanics and is used to approximate high-dimensional systems through a lower-dimensional one. It is the same idea as having the scalar temperature for a gas instead of keeping track of the kinetic energy of every single particle. The mean-field approach is a crude approximation in the sense that one assumes that every particle in the system only experiences the average behaviour of its neighbours. This average is bound to be different from the actual value which will fluctuate. According to the central limit theorem of statistics however, the more neighbours there are interacting the less the average will fluctuate and the closer the approximation will get to the truth.

Mean-field theory has successfully been used in neuroscience with one of the examples being the cortical model used in this report where a mean-field approximation has been applied on the Adaptive exponential integrate-and-fire neuron model resulting in the so called ALN model. There are a series of conditions that need to be fulfilled for the construction of this mean-field model: all the neurons within each population need to have the same properties, there needs to be a very large number of neurons and the connectivity needs to be sparse and random within each

population. For the derivation and additional assumptions see Cakan et al. [13].

2.3.3 Neurolib

Neurolib is an open-source framework for whole-brain modeling written in Python [12]. It provides several neural mass models, among them the cortical and thalamic models used in this report and soon the thalamocortical model which we have created by combining the two former mentioned models. The brain regions are connected to each other informed by empirical diffusion tensor imaging data [12]. Neurolib also contains many tools for extensive model analysis and optimization such as an evolutionary optimization module and a parameter exploration module.

3

Methods

All code in this project have been run using Python version 3.7.0 and Neurolib version 0.6.1.

3.1 Cortical model

The cortical model in neurolib is derived from applying mean-field theory to the exponential integrate-and-fire (AdEx) neurons which are explained in Section 2.3.1.4. The resulting model is called the ALN model and is represented by a node with an excitatory (E) and an inhibitory (I) population. In the following describing equations of the ALN model a general population is represented with an $\alpha \in \{E, I\}$. The output of interest from each population is the population spike rate r_α which is the average neural spiking for a population. It is computed for each timestep with a pre-computed transfer function $r_\alpha = \Phi_r(\mu_\alpha, \sigma_\alpha)$ with the dependent variables μ_α , which is the total mean membrane current and σ_α which is the membrane current variance. The dynamics of the membrane currents are given by the following equations:

$$\tau_\alpha \frac{d\mu_\alpha}{dt} = \mu_\alpha^{\text{syn}}(t) + \mu_\alpha^{\text{ext}}(t) + \mu_\alpha^{\text{ou}}(t) - \mu_\alpha(t) \quad (3.1)$$

$$\sigma_\alpha^2(t) = \sum_{\beta \in \{E, I\}} \frac{2J_{\alpha\beta}^2 \sigma_{s,\alpha\beta}^2(t) \tau_{s,\beta} \tau_m}{(1 + r_{\alpha\beta}(t)) \tau_m + \tau_{s,\beta}} + \sigma_{\text{ext},\alpha}^2 \quad (3.2)$$

Equation 3.2 describes the dynamics of the variance σ_α^2 of the membrane currents containing the input-dependent adaptive timescale $\tau_\alpha = \Phi_\tau(\mu_\alpha, \sigma_\alpha)$ which is calculated from a precomputed transfer function (see [11]). In equation 3.1 we have μ_α which is the total mean membrane current, μ_α^{ext} the currents from external input sources, μ_α^{ou} the external noise input and μ_α^{syn} the currents induced by synaptic activity. The dynamics of this synaptic current μ_α^{syn} are in turn given by:

$$\mu_\alpha^{\text{syn}}(t) = J_{\alpha E} \bar{s}_{\alpha E}(t) + J_{\alpha I} \bar{s}_{\alpha I}(t) \quad (3.3)$$

The parameters $J_{\alpha\beta}$ determine the maximum synaptic current when all synapses from population β to population α are active and $\bar{s}_{\alpha\beta}$ represents the mean of the fraction of all active synapses bounded between 0 (no active synapses) and 1 (all synapses active). Like α , β is either E or I . The synaptic dynamics are given by:

$$\frac{d\bar{s}_{\alpha\beta}}{dt} = \tau_{s,\beta}^{-1} ((1 - \bar{s}_{\alpha\beta}(t)) \cdot r_{\alpha\beta}(t) - \bar{s}_{\alpha\beta}(t)), \quad (3.4)$$

$$\frac{d\sigma_{s,\alpha\beta}^2}{dt} = \tau_{s,\beta}^{-2} \left((1 - \bar{s}_{\alpha\beta}(t))^2 \cdot \rho_{\alpha\beta}(t) + (\rho_{\alpha\beta}(t) - 2\tau_{s,\beta} (r_{\alpha\beta}(t) + 1)) \cdot \sigma_{s,\alpha\beta}^2(t) \right). \quad (3.5)$$

At every timestep – taking into account the input delay between nodes – one has the mean $r_{\alpha\beta}$ and the variance $\rho_{\alpha\beta}$ of the effective input rate from population β to α for a spike transmission delay d_α given by:

$$r_{\alpha\beta}(t) = \frac{c_{\alpha\beta}}{J_{\alpha\beta}} \tau_{s,\beta} \left(K_\beta \cdot r_\beta(t - d_\alpha) + \delta_{\alpha E} \delta_{\beta E} \cdot K_{gl} \sum_{j=0}^N C_{ij} \cdot r_\beta(t - D_{ij}) \right), \quad (3.6)$$

$$\rho_{\alpha\beta}(t) = \frac{c_{\alpha\beta}^2}{J_{\alpha\beta}^2} \tau_{s,\beta}^2 \left(K_\beta \cdot r_\beta(t - d_\alpha) + \delta_{\alpha E} \delta_{\beta E} \cdot K_{gl} \sum_{j=0}^N C_{ij}^2 \cdot r_\beta(t - D_{ij}) \right). \quad (3.7)$$

$r_\alpha(t)$ is the instantaneous population spike rate, $c_{\alpha\beta}$ defines the amplitude of the post-synaptic current caused by a single spike, K_{gl} is the global coupling strength parameter, $C_{i,j}$ gives the connection strength from region j to region i . and $D_{i,j}$ in the same way gives the delay from region j to region i . The Kronecker deltas restrict the inter-areal coupling to only be between excitatory subpopulations since the summation term is only non-zero when $\alpha = \beta = E \implies \delta_{\alpha E} \delta_{\beta E} = 1$.

3.1.1 Noise input μ_α^{ou} in cortical model

As can be seen in equation 3.1 every population α contains a contribution from $\mu_\alpha^{\text{ou}}(t)$ which is an independent noise input. It represents other not included neural sources such as subcortical brain areas and it is modeled as an Ornstein-Uhlenbeck process with a zero mean:

$$\frac{d\mu_\alpha^{\text{ou}}}{dt} = -\frac{\mu_\alpha^{\text{ou}}}{\tau_{ou}} + \sigma_{ou} \cdot \xi(t), \quad (3.8)$$

where $\xi(t)$ is a white noise process sampled from a normal distribution with zero mean and unit variance.

3.2 Thalamic model

The thalamic model consists of two populations, the excitatory thalamocortical neurons (TCR) and the inhibitory thalamic reticular nucleus (TRN). Like the cortical model the variable which is iterated over is the mean membrane potential which then is converted to firing rate with the following sigmoidal transfer function,

$$r(V) = \frac{r_{\max}}{1 + \exp(-(V - \theta)/\sigma)}, \quad (3.9)$$

containing the maximum firing rate r_{max} , firing threshold θ , and gain coefficient σ . For a thalamic population $\alpha \in \{t, r\}$, the mean membrane potential V_α is given by

$$\tau \dot{V}_\alpha = -(V_\alpha - E_{leak}) - w_e s_{e\alpha} (V_\alpha - E_e) - w_i s_{i\alpha} (V_\alpha - E_i) - C_m^{-1} \tau I^{\text{intrinsic}}. \quad (3.10)$$

where w_e, w_i are the synaptic input rates scaling the corresponding synaptic inputs s_e, s_i for excitatory (e) and inhibitory (i) synapses. E_e, E_i are the Nernst reversal potentials. The final term contains the additional intrinsic currents present, with τ being the membrane time constant and C_m the membrane capacitance. The additional intrinsic currents vary slightly between TCR and TRN, both of them include a potassium leak current

$$I_{LK} = g_{LK} (V - E_K), \quad (3.11)$$

and a T-type calcium current,

$$I_T = g_T m_\infty^2 h (V - E_{Ca}) \quad (3.12)$$

In these equations g_{LK} and g_T are the conductances of each intrinsic current, E_K and E_{Ca} their Nernst reversal potentials and m_∞^2 and h are the gating functions of the T-type calcium current. Additionally the TCR population contains what is called an anomalous rectifying current I_h :

$$I_h = g_h (m_{h1} + g_{inc} m_{h2}) (V - E_h) \quad (3.13)$$

where g_h is its conductance, E_h its Nernst reversal potential, m_{h1} and m_{h2} the gating functions and finally the conductivity scaling g_{inc} . This rectifying current I_h gives rise to the waxing and waning of spindle oscillations in a single isolated thalamus. So taken altogether $I^{\text{intrinsic}} = I_t^{LK} + I_t^T + I_h$ for TCR and $I^{\text{intrinsic}} = I_r^{LK} + I_r^T$ for TRN.

The synaptic transmission from the firing population k' to the receiving population k in the thalamic model is described by

$$s_{lk}(t) = \sum_{k'} \alpha_l(t) \otimes N_{kk'} r_{k'}(t) + \phi'(t) \quad (3.14)$$

here $l \in \{e, i\}$ where $l = e$ corresponds to being an excitatory AMPA synapse whilst $l = i$ corresponds to an inhibitory GABA synapse. $N_{kk'}$ is the connection strength from population k' to k , $\phi'(t)$ is background noise input and \otimes is the convolution operator. $\alpha_l(t)$ is an alpha function representing the synaptic response to a single spike, it is given by

$$\alpha_l(t) = \gamma_l^2 \cdot t \cdot \exp(-\gamma_l t) \quad (3.15)$$

where γ_l is the decay constant of the synaptic response. The convolution in equation 3.14 is replaced by a second-order ordinary differential equation for easier numerical calculation which results in:

$$\ddot{s}_{lk} = \gamma_l^2 \left(\sum_{k'} N_{kk'} r_{k'}(t) + \phi'(t) - s_{lk}(t) \right) - 2\gamma_l \dot{s}_{lk}(t) \quad (3.16)$$

Its background noise input $\phi'(t)$ is modeled as an Ornstein-Uhlenback process with zero drift and finite variance. As in the cortical model the noise represents other neural processes not accounted for in the model such as input from other brain regions. [30, 20]

3.3 Thalamocortical model

This section shows the equations for how the thalamus and the cortical model were connected in order to create the thalamocortical model.

3.3.1 Connection thalamus \rightarrow cortex

The firing rate of the thalamus enters the cortical model in equation 3.6 and 3.7 where the summation now goes over the N cortical nodes and finally also the thalamic node with index $N + 1$ giving rise to the slightly modified equations 3.6' and 3.7':

$$r_{\alpha\beta}(t) = \frac{c_{\alpha\beta}}{J_{\alpha\beta}} \tau_{s,\beta} \left(K_{\beta} \cdot r_{\beta}(t - d_{\alpha}) + \delta_{\alpha E} \delta_{\beta E} \cdot K_{gl} \sum_{j=0}^{N+1} C_{ij} \cdot r_{\beta}(t - D_{ij}) \right), \quad (3.6')$$

$$\rho_{\alpha\beta}(t) = \frac{c_{\alpha\beta}^2}{J_{\alpha\beta}^2} \tau_{s,\beta}^2 \left(K_{\beta} \cdot r_{\beta}(t - d_{\alpha}) + \delta_{\alpha E} \delta_{\beta E} \cdot K_{gl} \sum_{j=0}^{N+1} C_{ij}^2 \cdot r_{\beta}(t - D_{ij}) \right). \quad (3.7')$$

3.3.2 Connection cortex \rightarrow thalamus

The firing rate of the cortical nodes enters the thalamus in equation 3.16 in the excitatory case ($l = e$) for both the excitatory ($k = t$) and inhibitory ($k = r$) population:

$$\ddot{s}_{et} = \gamma_e^2 \left(\sum_{k'} N_{tk'} r_{k'}(t) + \phi'(t) + \sum_{j=0}^N C_{ij} \cdot r_{\beta}(t - D_{ij}) - s_{et}(t) \right) - 2\gamma_e \dot{s}_{et}(t) \quad (3.16t)$$

$$\ddot{s}_{er} = \gamma_e^2 \left(\sum_{k'} N_{rk'} r_{k'}(t) + \phi'(t) + \sum_{j=0}^N C_{ij} \cdot r_{\beta}(t - D_{ij}) - s_{er}(t) \right) - 2\gamma_e \dot{s}_{er}(t) \quad (3.16r)$$

where the new summation term is added including the firing rate from the N cortical nodes ($N = 1$ or $N = 80$).

3.4 Node connections in a 80+1-node whole-brain model

In order to simulate an 80 + 1-node model the connectivity (i.e. weighting of input) and delay from each node to every other node needs to be specified. A practical way of encoding this information is through 81×81 connectivity and delay matrices, where element of index i, j represents the connection strength/delay from the j th node to the i th node. Such a connectivity and delay matrix are included in Neurolib. This structural connectivity and delay is based on a probabilistic DTI tractography and the different regions defining each node are based on the AAL2 atlas. The AAL2 atlas — and therefore also the data available in Neurolib — contains two thalamic

nodes corresponding to the left and right side of the thalamus. The computational model of the thalamus we have used is a single node model of the complete thalamus, to reconcile this we have therefore averaged the connections and delays of the two thalamic halves to get the connections and delays for our single thalamic node.

3.5 Signal analysis

The output data analysed was a time series of mean firing rate which both was converted into its power spectrum and searched for different characteristics, the tools and techniques for doing this are described in more detail below.

3.5.1 EEG Dataset

The MPI-LEMON EEG dataset was used to make comparisons between simulated data and data from real humans [7]. The dataset is publicly available and contains data from 227 participants. The participants were both men and women of different ages (see description paper [7] for more detailed information).

3.5.2 Power spectrums

Power spectrums (or power spectral density) were approximated from the firing rates using the scipy implementation of Welch's method with parameter window set to "hanning". The power spectral density is the Fourier transform of the autocorrelation function [26].

The power spectrums were compared in different ways. They were compared qualitatively, for example by looking at the shape and peaks of the spectrum. They were also compared quantitatively by calculating the correlation between the power spectrum retrieved from the dataset and the power spectrum retrieved from the simulations. Lastly they were also compared quantitatively by detecting peaks in the power spectrums and comparing the frequency and height of the peaks. In the last case the `find_peaks` function from scipy was used with a threshold on the lowest accepted prominence.

3.5.3 Summary statistics

A number of values were calculated from the time series and from the power spectrums for the analysis. The ones that are presented in the results are the difference between the minimum and maximum value of a time series, the mean value of a time series and The prominence of peaks. Prominence is defined as the vertical distance between a peak and its lowest contour line.

3.5.4 Spindles

To detect spindles the same technique as in Jaycay et al. [20] was used. In other words the A7 spindle detection algorithm described in Lacourse et al. [24] with the

same modifications as in Jaycay et al.

3.6 Parameter search

In order to understand how different parameters affected the output of the model parameter searches were run. To be able to visualize them in a reasonable way, only parameter searches involving one or two parameters were run. The parameters that were examined in the parameter searches were b , w_e^r , w_i^r , w_e^t , w_i^t and g_{LK} and the choice of parameters was based on the findings of Krishnan et al.

4

Results

4.1 Thalamocortical implementation

The thalamocortical model implemented in this project was 12 times faster than the already existing thalamus-cortex model in Neurolib implemented in the Neurolib framework ‘Multimodel’. For the benchmarking the models were setup to run a simulation of 10000 ms with a timestep of 0.01 ms. After 100 runs the mean and standard deviation of the thalamocortical model were 252 ms with 0.688 ms standard deviation whilst the multimodel implementation had a mean runtime of 3040 ms with a standard deviation of 11.4 ms. The benchmarking was performed on a AMD Ryzen 9 5900HX processor.

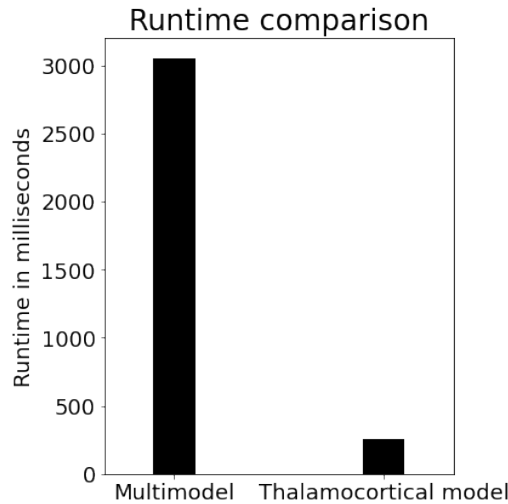


Figure 4.1: Runtimes of the existing thalamus-cortex implementation in Neurolib Multimodel compared to the implemented thalamocortical model. The thalamocortical model was an order of magnitude faster taking only 8.3% of the time the multimodel took with the runtime mean and standard deviations being 252 ± 0.688 ms compared to 3040 ± 11.4 ms. The runtime statistics were calculated after 100 runs with the models running a 10000 ms simulation with the timestep of 0.1 ms.

4.2 2-node model

4.2.1 Sleeping state

The results in this section are generated using parameters from tables A.1, A.2 and A.3 in Appendix A.1 which are based on the results of Jaycay et al. [20].

A 20 second time excerpt of the firing rate of the excitatory population in the cortical node and the thalamocortical relay population in the thalamic node are shown in Figure 4.2 and 4.3 respectively. The power spectrum of the firing rate of the excitatory population in the cortical node from a 120 second simulation is shown in Figure 4.4.

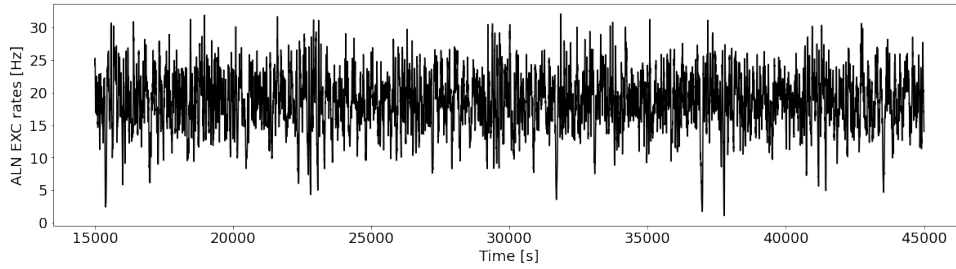


Figure 4.2: The figure shows a 20 second time excerpt of the firing rate of the excitatory population in the cortical node. The simulation was run with one cortical and one thalamic node with parameters from tables A.1, A.2 and A.3 in Appendix A.1.

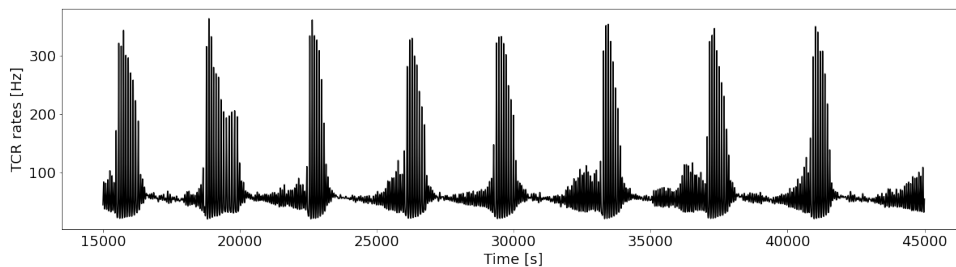


Figure 4.3: The figure shows a 20 second time excerpt of the firing rate of the thalamocortical relay population in the thalamic node. The simulation was run with one cortical and one thalamic node with parameters from tables A.1, A.2 and A.3 in Appendix A.1.

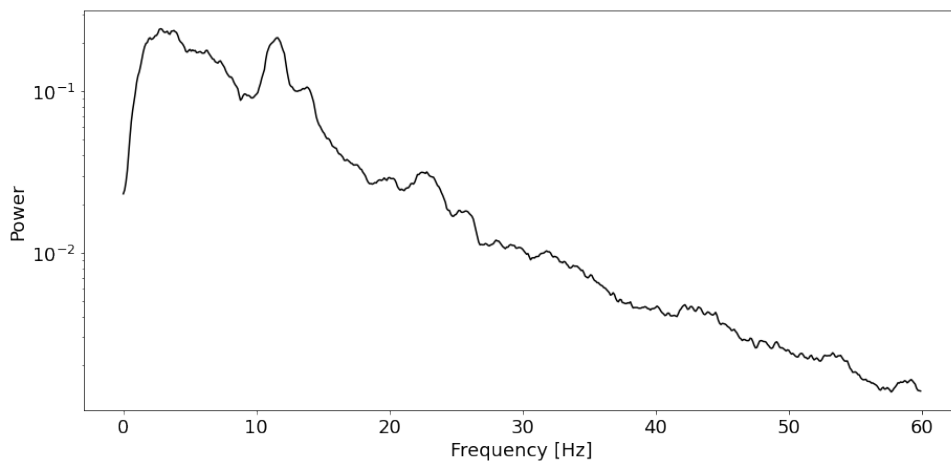


Figure 4.4: The figure shows the power spectrum of the firing rate in the excitatory population from a 120 second simulation. The simulation was run with one cortical and one thalamic node with parameters from tables A.1, A.2 and A.3 in Appendix A.1.

4.2.2 Awake state

In this section results from the attempts to simulate the model in an awake state using one cortical and one thalamic node will be presented. All parameter searches in this section uses parameters from tables A.1, A.2 and A.3 in Appendix A.1 which are based on the results of Jaycay et al. [20] as starting point.

4.2.2.1 Exploration of individual parameters

Results in this section are from parameter searches where only one parameter were varied at a time.

Graphs showing the frequency of the most prominent peak in a power spectrum between 7.5 Hz and 15 Hz of the firing rate in the excitatory population in the cortical node from a 120 second simulation for varying values of w_i^r and w_i^t are shown in Figure 4.5 and 4.6 respectively.

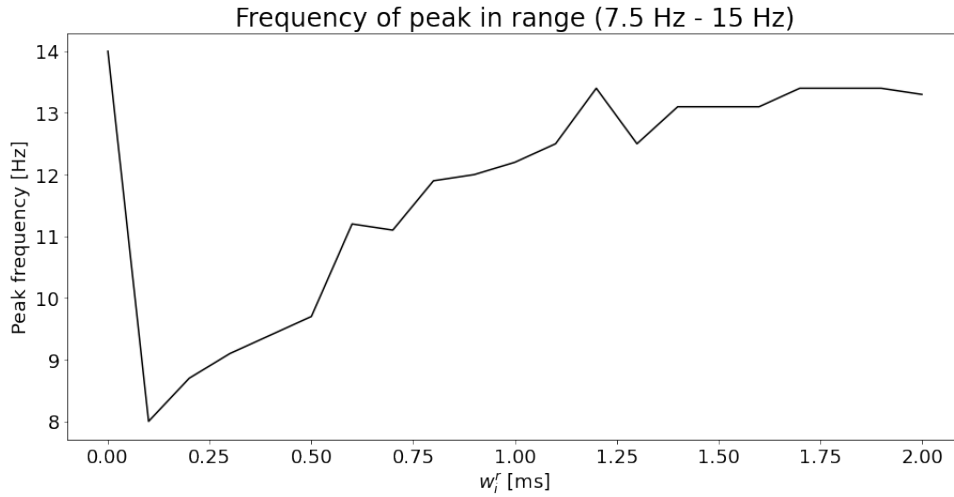


Figure 4.5: The figure shows the frequency of the most prominent peak in a power spectrum between 7.5 Hz and 15 Hz of the firing rate in the excitatory population in the cortical node from a 120 second simulation for varying values of w_i^r . The simulations were run with one cortical and one thalamic node with parameters from tables A.1, A.2 and A.3 in Appendix A.1 as starting point. Note that the frequency of the peak varies substantially over the range.

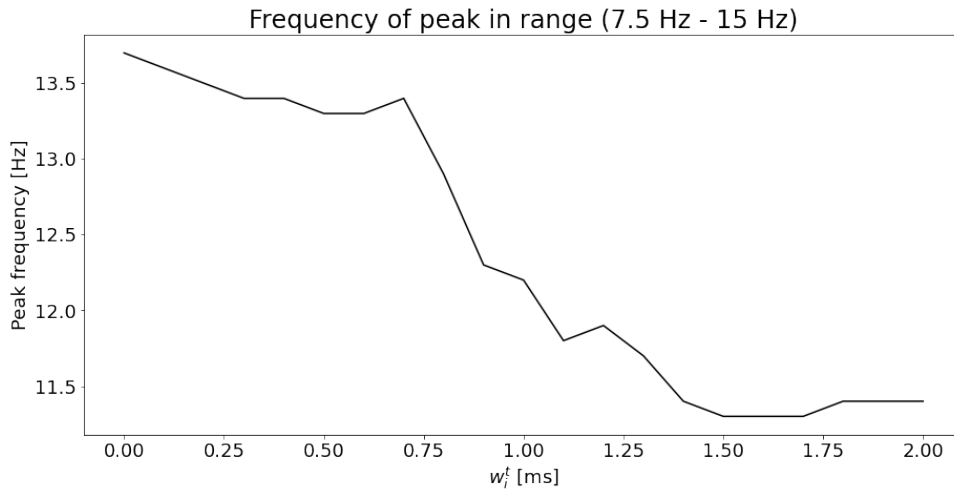


Figure 4.6: The figure shows the frequency of the most prominent peak in a power spectrum between 7.5 Hz and 15 Hz of the firing rate in the excitatory population in the cortical node from a 120 second simulation for varying values of w_i^t . The simulations were run with one cortical and one thalamic node with parameters from tables A.1, A.2 and A.3 in Appendix A.1 as starting point. Note that the frequency of the peak varies substantially over the range.

A 20 second time excerpt of the firing rate of the thalamocortical relay population in the thalamic node with $w_i^r = 0.5$ is shown in Figure 4.7. The power spectrum, from a 120 second simulation, of the firing rate of the excitatory population in the cortical node is shown in Figure 4.8.

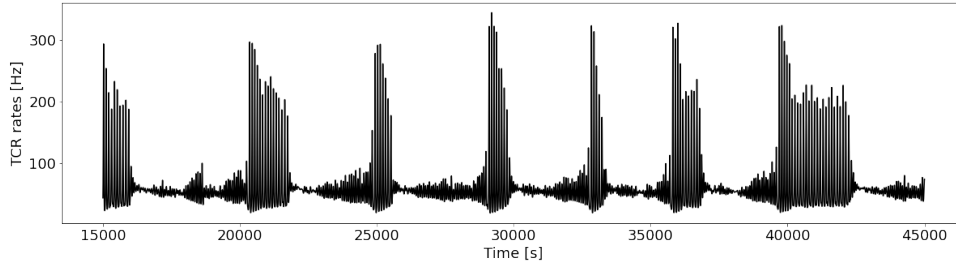


Figure 4.7: The figure shows a 20 second time excerpt of the firing rate of the thalamocortical relay population in the thalamic node. The simulation was run with one cortical and one thalamic node with $w_i^r = 0.5$. The rest of the parameters are from tables A.1, A.2 and A.3 in Appendix A.1.

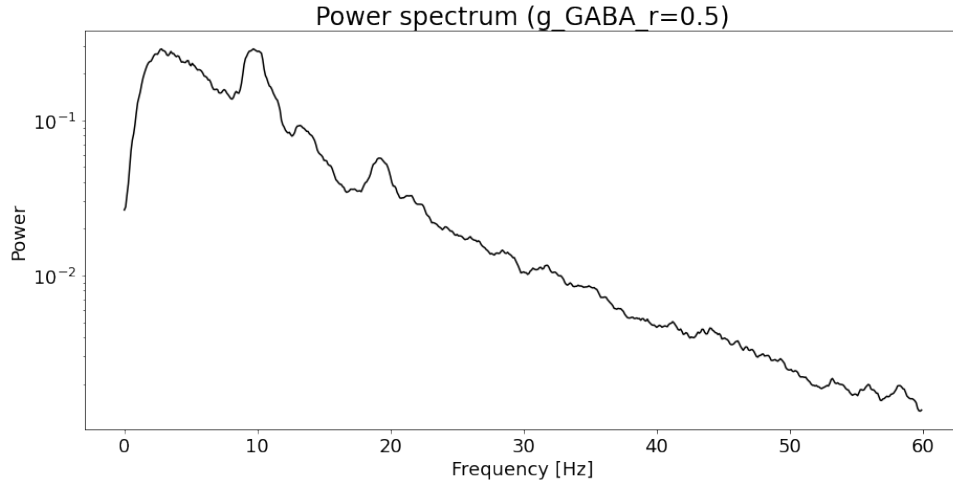


Figure 4.8: The figure shows the power spectrum of the firing rate in the excitatory population in the cortical node from a 120 second simulation. The simulation was run with one cortical and one thalamic node with $w_i^r = 0.5$. The rest of the parameters are from tables A.1, A.2 and A.3 in Appendix A.1. Note the peak at about 10 Hz.

4.2.2.2 Exploration of two parameters at a time

The difference between the maximum and the minimum value of the firing rate of the thalamocortical relay population in the thalamic node is shown in Figure 4.9. The average spindle amplitude of the firing rate of the thalamocortical relay population in the thalamic node is shown in Figure 4.10. The prominence of the most prominent peak in a power spectrum between 8 Hz and 12 Hz of the firing rate in the excitatory population in the cortical node is shown in Figure 4.11. All of these values were calculated from 120 second simulations for varying values of w_i^r and w_i^t .

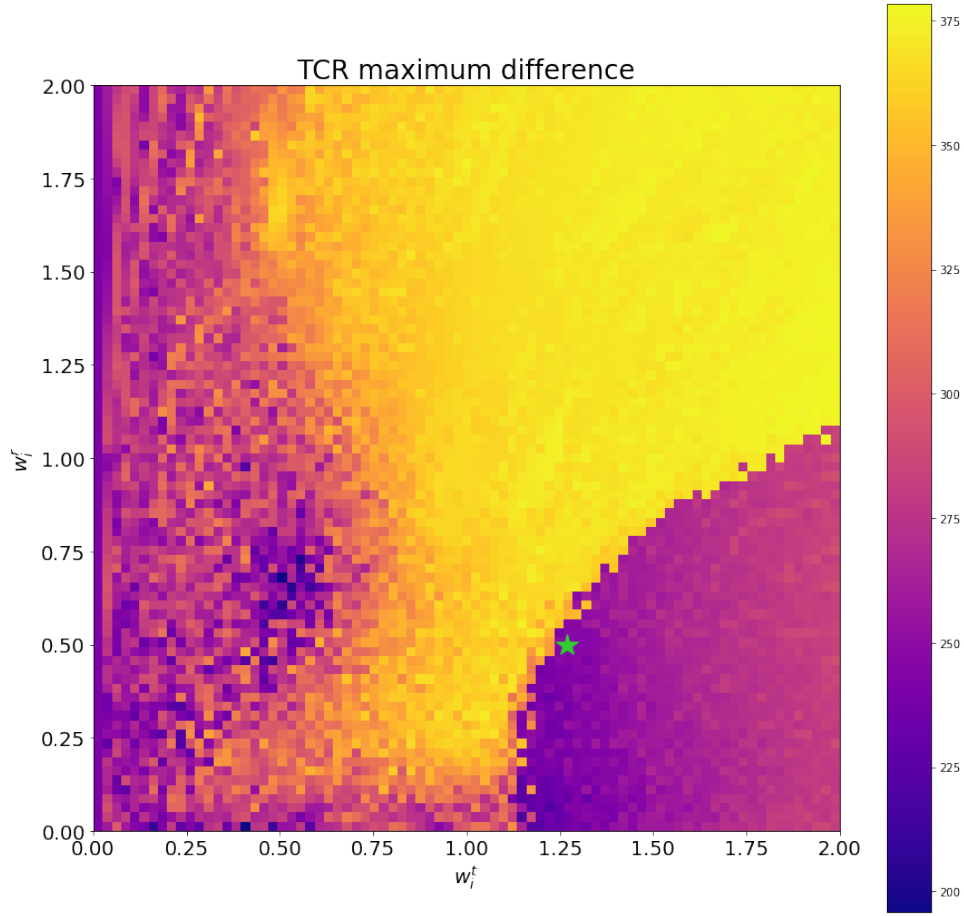


Figure 4.9: The figure shows the difference between the maximum and the minimum value of the firing rate of the thalamocortical relay population in the thalamic node from a 120 second simulation, for varying values of w_i^r and w_i^t . The rest of the parameters are from tables A.1, A.2 and A.3 in Appendix A.1. $w_i^t = 1.27, w_i^r = 0.5$ is marked with a green star.

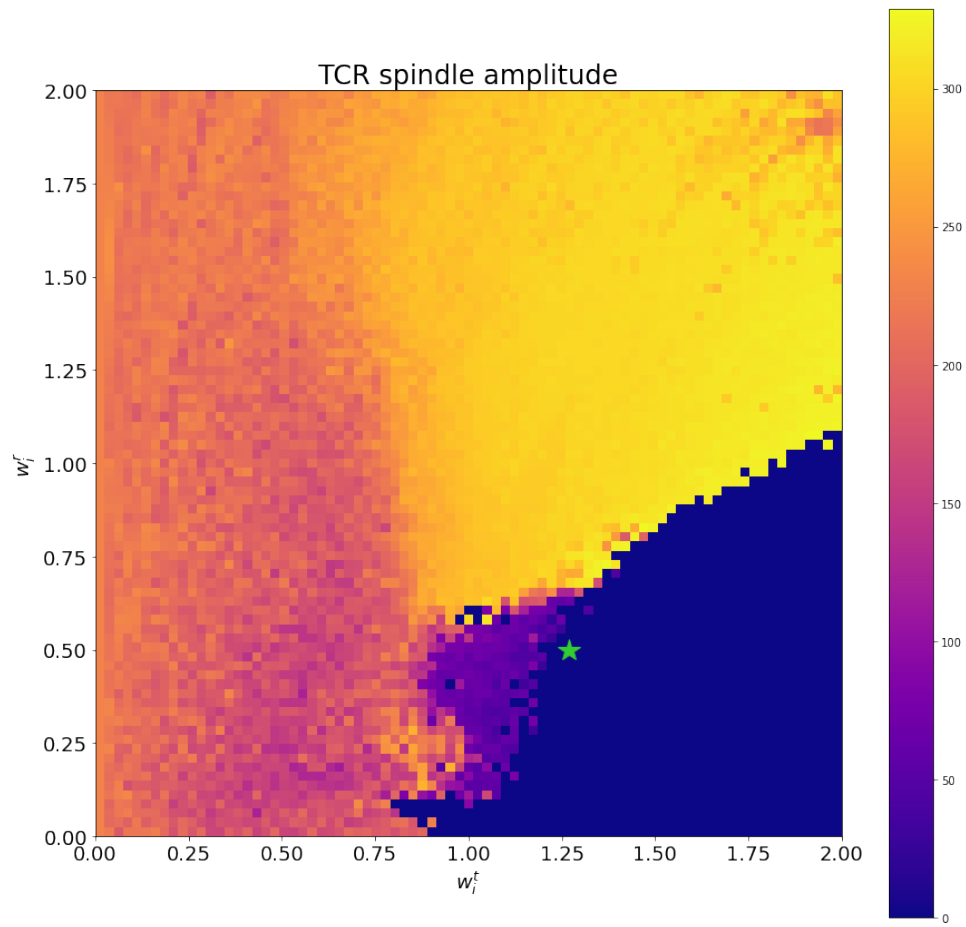


Figure 4.10: The figure shows the average spindle amplitude of the firing rate of the thalamocortical relay population in the thalamic node from a 120 second simulation, for varying values of w_i^r and w_i^t . The rest of the parameters are from tables A.1, A.2 and A.3 in Appendix A.1. $w_i^t = 1.27, w_i^r = 0.5$ is marked with a green star.

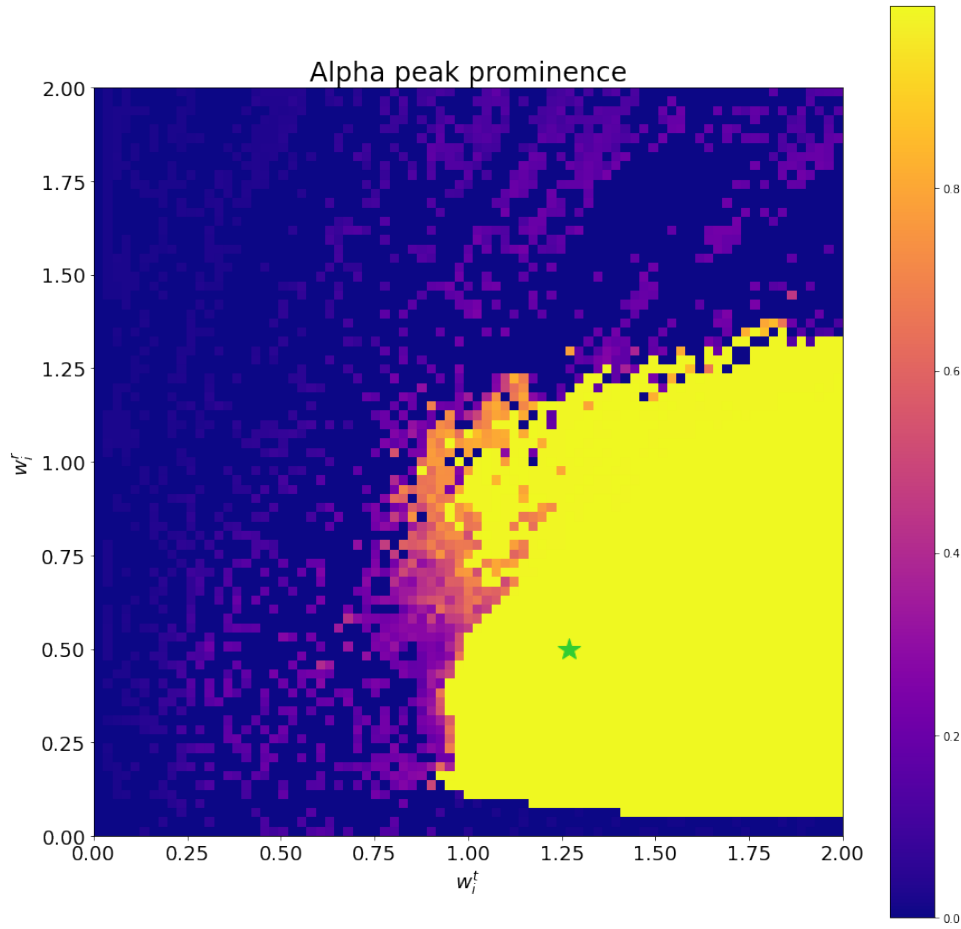


Figure 4.11: The figure shows the prominence of the most prominent peak in the range 8Hz to 12Hz in a power spectrum of the firing rate in the excitatory population in the cortical node from a 120 second simulation, for varying values of w_i^r and w_i^t . The rest of the parameters are from tables A.1, A.2 and A.3 in Appendix A.1. $w_i^t = 1.27, w_i^r = 0.5$ is marked with a green star.

A 20 second time excerpt of the firing rate of the excitatory population in the cortical node and a 20 second time excerpt of the thalamocortical relay population in the thalamic node are shown in Figure 4.12 and 4.13 respectively. The power spectrum of the firing rate of the excitatory population in the cortical node from a 120 second simulation is shown in Figure 4.14. All were run with $w_i^t = 1.27, w_i^r = 0.5$.

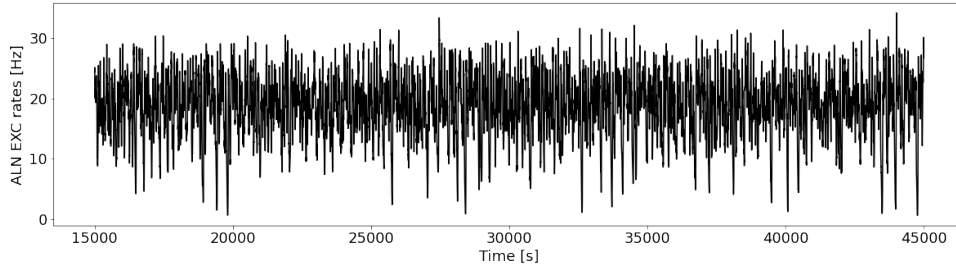


Figure 4.12: The figure shows a 20 second time excerpt of the firing rate of the excitatory population in the cortical node. The simulation was run with one cortical and one thalamic node with $w_i^t = 1.27, w_i^r = 0.5$. The rest of the parameters are from tables A.1, A.2 and A.3 in Appendix A.1.

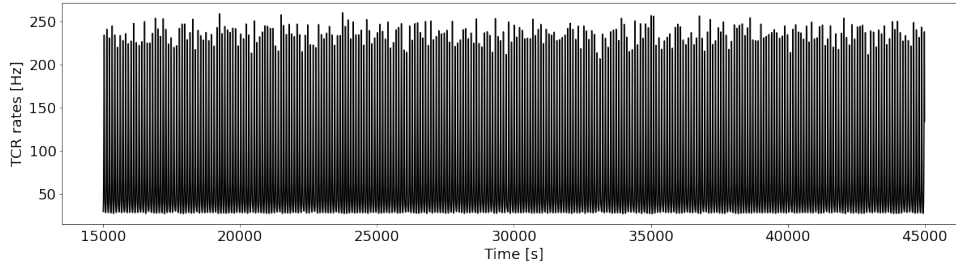


Figure 4.13: The figure shows a 20 second time excerpt of the firing rate of the thalamocortical relay population in the thalamic node. The simulation was run with one cortical and one thalamic node with $w_i^t = 1.27, w_i^r = 0.5$. The rest of the parameters are from tables A.1, A.2 and A.3 in Appendix A.1.

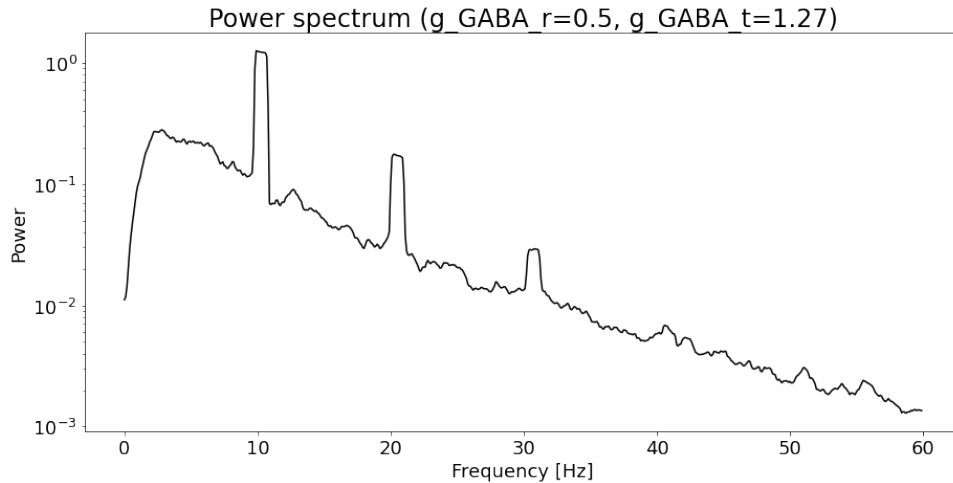


Figure 4.14: The figure shows the power spectrum of the firing rate in the excitatory population in the cortical node from a 120 second simulation. The simulation was run with one cortical and one thalamic node with $w_i^t = 1.27, w_i^r = 0.5$. The rest of the parameters are from tables A.1, A.2 and A.3 in Appendix A.1. Note the peak at about 10 Hz.

4.3 81-node model

The results in this section are generated using parameters from Table A.4 in Appendix A.1.1 which are based on the results of Cakan et al. [11]. The other parameters are from tables A.1, A.2 and A.3 in Appendix A.1 which are based on the results of Jaycay et al. [20]. All simulations in this section are run with scaling values of connection strengths $c_{ctx-ctx} = 1$, $c_{ctx-thal} = 2$, $c_{thal-ctx} = 10$.

4.3.1 Sleeping state

The spindling frequency (the frequency of UP states) of the firing rates of thalamocortical relay population in the thalamic node is shown in Figure 4.15. The mean value in the range 7.5 Hz to 15 Hz of the mean power spectrum of the firing rates of the excitatory populations in the cortical nodes is shown in Figure 4.16. All of these values were calculated from 60 second simulations for varying values of b and μ_E .

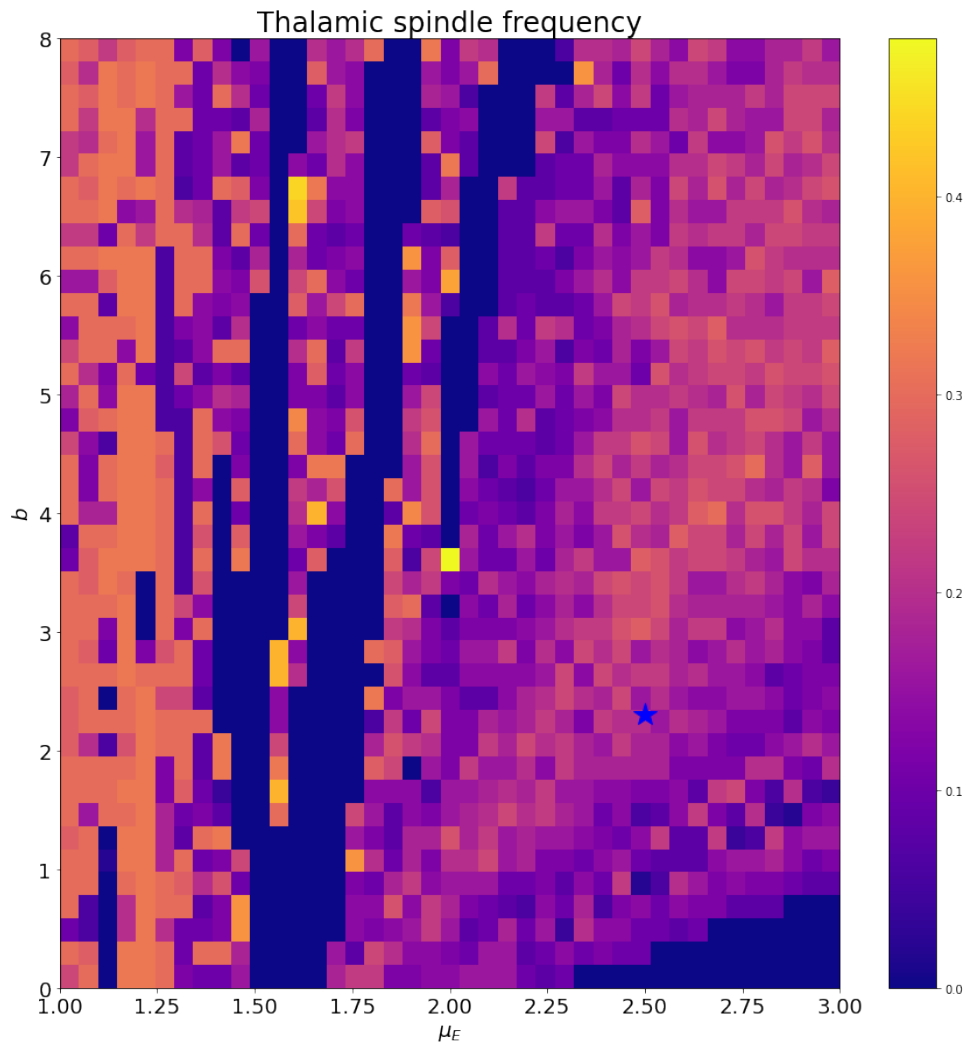


Figure 4.15: The figure shows the spindling frequency of the firing rates of thalamocortical relay population in the thalamic node from a 60 second simulation, for varying values of b and μ_E . Parameters are from Table A.4 in Appendix A.1.1. The other parameters are from tables A.1, A.2 and A.3 in Appendix A.1. $\mu_{ext_mean} = 2.5, b = 2.3$ is marked with a blue star.

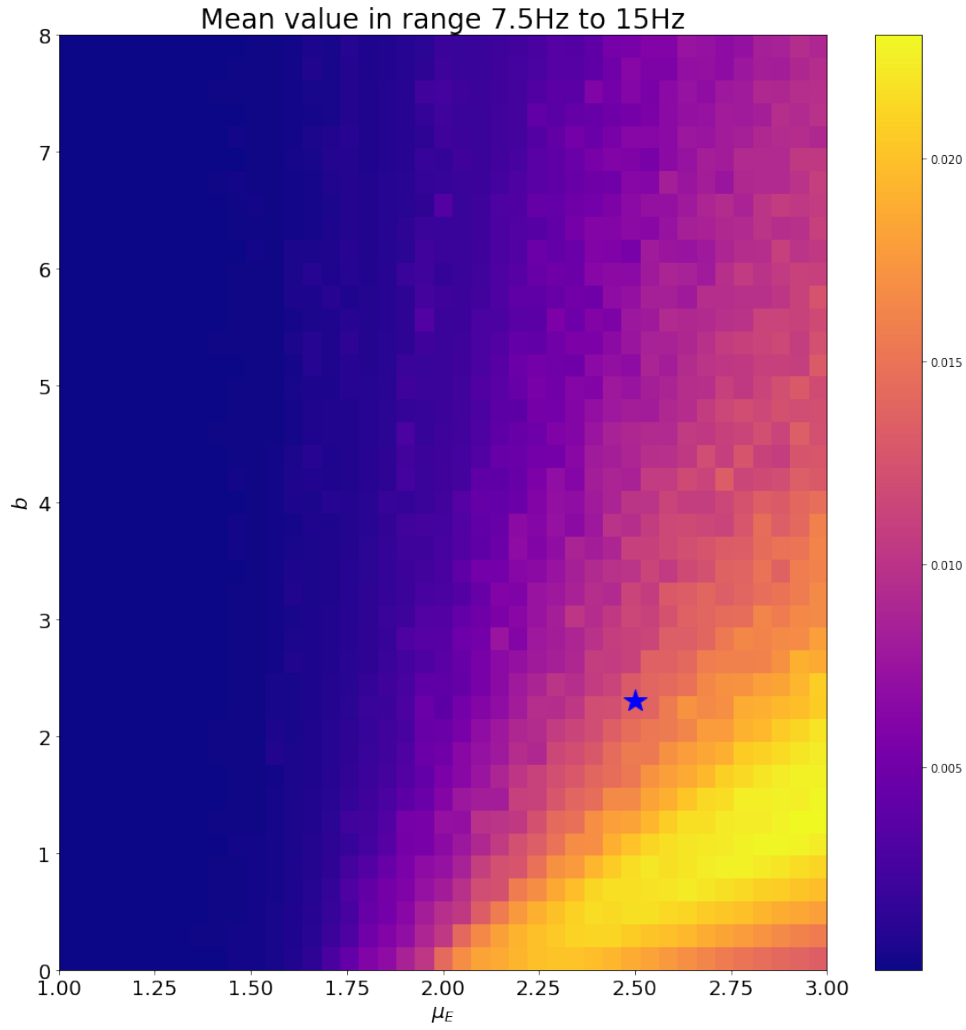


Figure 4.16: The figure shows the mean value in the range 7.5Hz to 15Hz of the mean power spectrum of the firing rates of the excitatory populations in the cortical nodes from a 60 second simulation, for varying values of b and μ_E . Table A.4 in Appendix A.1.1. The other parameters are from tables A.1, A.2 and A.3 in Appendix A.1. $\mu_{E_ext_mean} = 2.5, b = 2.3$ is marked with a blue star.

A 20 second time excerpt of the average firing rate of the excitatory populations in the 80 cortical nodes and a 20 second time excerpt of the thalamocortical relay population in the thalamic node are shown in Figure 4.17 and 4.18 respectively. The mean power spectrum of the firing rate of the excitatory populations in the 80 cortical nodes from a 120 second simulation is shown in Figure 4.19.

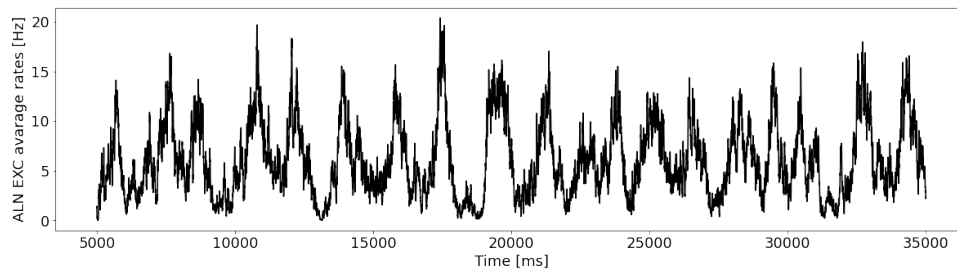


Figure 4.17: The figure shows a 20 second time excerpt of the mean of the firing rate of the excitatory population in all 80 cortical nodes. The simulation was run with 80 cortical nodes and one thalamic node with parameters from Table A.4 in Appendix A.1.1. The other parameters are from tables A.1, A.2 and A.3 in Appendix A.1.

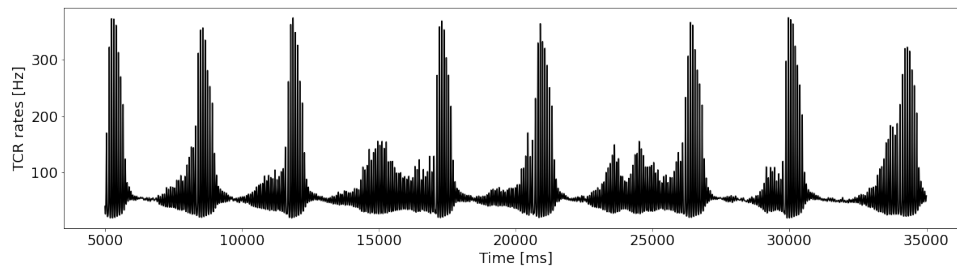


Figure 4.18: The figure shows a 20 second time excerpt of the firing rate of the thalamocortical relay population in the thalamic node. The simulation was run with 80 cortical nodes and one thalamic node with parameters from Table A.4 in Appendix A.1.1. The other parameters are from tables A.1, A.2 and A.3 in Appendix A.1.

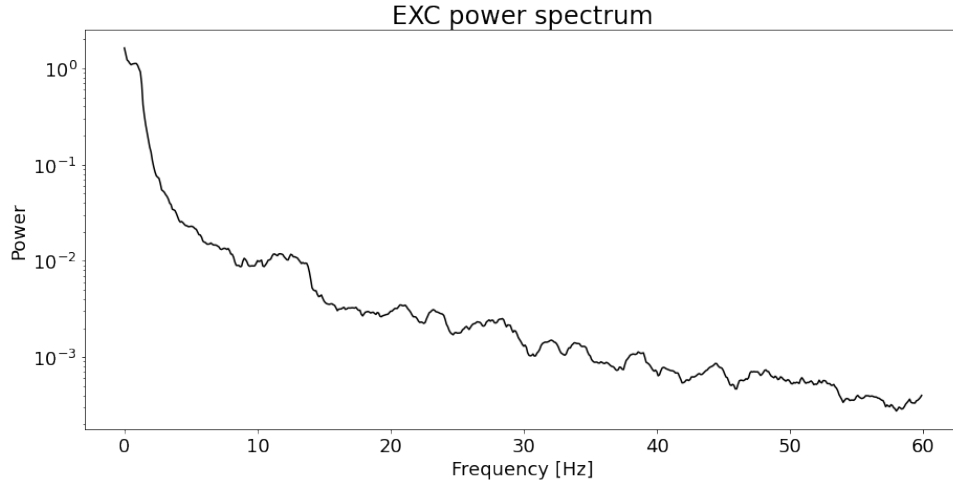


Figure 4.19: The figure shows the mean power spectrum of the firing rate in the excitatory population in all cortical nodes from a 120 second simulation. The simulations were run with 80 cortical nodes and one thalamic node with parameters from Table A.4 in Appendix A.1.1. The other parameters are from tables A.1, A.2 and A.3 in Appendix A.1. Note the peak at about 10 Hz.

4.3.2 Awake state

A 20 second time excerpt of the average firing rate of the excitatory populations in the 80 cortical nodes and a 20 second time excerpt of the thalamocortical relay population in the thalamic node are shown in Figure 4.20 and 4.20 respectively. The mean power spectrum of the firing rate of the excitatory populations in the 80 cortical nodes from a 120 second simulation is shown in Figure 4.22. All were run with $w_i^t = 1.27$, $w_i^r = 0.5$.

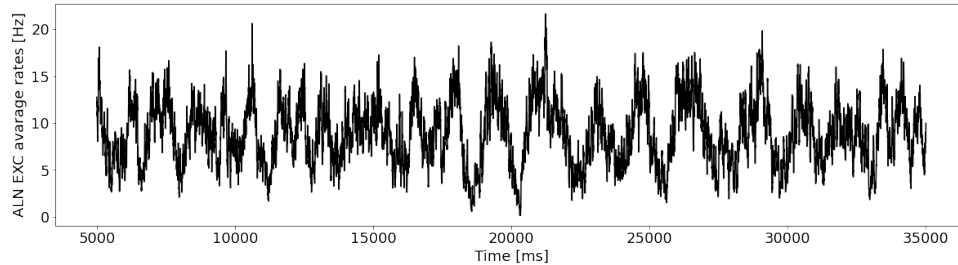


Figure 4.20: The figure shows a 20 second time excerpt of the mean of the firing rate of the excitatory populations in all 80 cortical nodes. The simulation was run with 80 cortical nodes and one thalamic node with $w_i^t = 1.27$, $w_i^r = 0.5$ and with parameters from Table A.4 in Appendix A.1.1. The other parameters are from tables A.1, A.2 and A.3 in Appendix A.1.

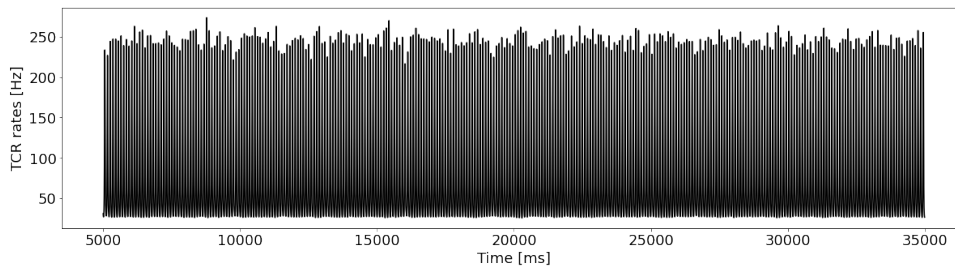


Figure 4.21: The figure shows a 20 second time excerpt of the firing rate of the thalamocortical relay population in the thalamic node. The simulation was run with 80 cortical nodes and one thalamic node with $w_i^t = 1.27, w_i^r = 0.5$ and with parameters from Table A.4 in Appendix A.1.1. The other parameters are from tables A.1, A.2 and A.3 in Appendix A.1.

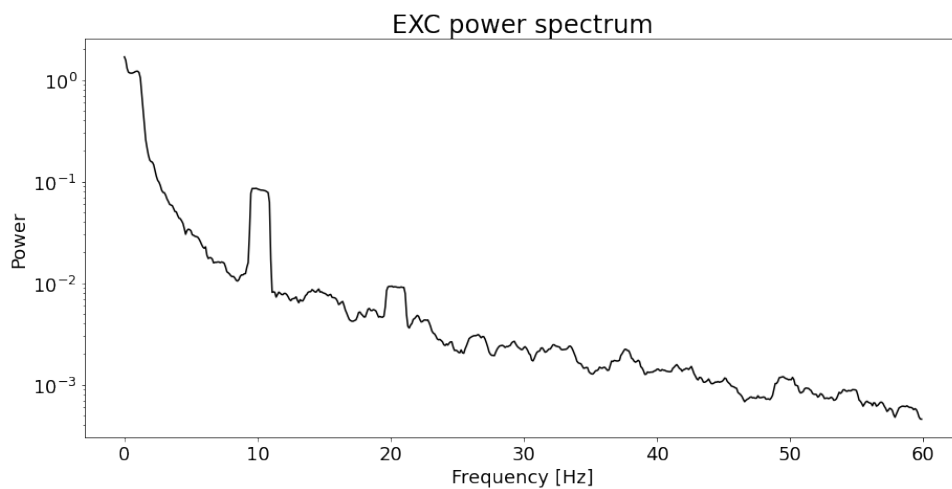


Figure 4.22: The figure shows the mean power spectrum of the firing rate in the excitatory populations in all cortical nodes from a 120 second simulation. The simulation was run with 80 cortical nodes and one thalamic node with $w_i^t = 1.27, w_i^r = 0.5$ and with parameters from Table A.4 in Appendix A.1.1. The other parameters are from tables A.1, A.2 and A.3 in Appendix A.1. Note the peak at 10 Hz.

5

Discussion

5.1 2-node model

5.1.1 Sleeping state

The parameters to generate the sleeping state were taken from Jaycay et al. [20]. The figures 4.2, 4.3 and 4.4 look qualitatively similar to the results in Jaycay et al. There are similar downstates observable in the cortical firing rates. The spindles in the thalamic firing rates are similar in height, frequency and length. And the power spectrum of the cortical firing rates have similar shape and peaks.

5.1.2 Awake state

The major feature we were looking for when trying to model the neural dynamics in an awake state was an alpha peak. Parameter searches were carried out for this purpose. The parameters that we chose to investigate were the parameters that were changed in Krishnan et al. [23] to perform state changes of their model.

5.1.2.1 Exploration of individual parameters

We were looking for parameters that when changed would generate an alpha peak in the power spectrum of the cortical firing rates and/or generate non-spindling firing rates in the thalamic node. No parameters on their own would generate both of these phenomena. However a number of them strongly affected the spindling or the frequency of the peak. b affected spindling. w_e^r , w_i^r , w_e^t and w_i^t affected the frequency of the peak. g_{LK} affected the spindling.

Two parameters were found to generate an alpha peak. w_i^t and w_i^r shifted the peak observable in Figure 4.2 horizontally. This is visualized in Figures 4.5 and 4.6. However like mentioned changing these parameters did not generate a non-spindling state. An example of this is shown in Figures 4.7 and 4.8 where one can see a clear alpha peak in the power spectrum of the cortical firing rates but also spindling in the thalamic firing rates.

5.1.2.2 Exploration of two parameters at a time

When running parameter searches of two parameters at a time we were looking for the same state. To see where in parameter space spindling was occurring it was

helpful to look at the difference between the maximum and the minimum value of the thalamic firing rates (see Figure 4.9) and the average amplitude of the spindles (see Figure 4.10). To detect an alpha peak the prominence of the most prominent peak in the range 8Hz to 12 Hz was plotted for each pair of parameters (see Figure 4.11).

Not all possible pairs of parameters were investigated, only the ones that during the exploration of individual parameters showed to generate an alpha peak or a non-spindling state. The pair that was found to generate the clearest example of the desired features were w_i^t and w_i^r . As can be seen in Figures 4.9, 4.10 and 4.11 there is a large region where there is no spindling in the thalamic node while a strong alpha peak is visible in the power spectrum of the cortical node.

A point from the interesting region $w_i^t = 1.27, w_i^r = 0.5$, marked with a green star in Figures 4.9, 4.10 and 4.11.) is presented in more detail in Figures 4.12, 4.13 and 4.14. One can see that there is no spindling in the thalamic firing rates and that there is a clear peak in the correct range in the power spectrum of the cortical firing rates. However the peak is very thin and very prominent which is not how they look in a realistic power spectrum.

5.2 81-node model

5.2.1 Sleeping state

When trying to simulate the 81-node model in a sleeping state we had the same goals as in the two-node model. Parameters for the cortical nodes was taken from Cakan et al. [11] while parameters for the thalamic node was taken from Jaycay et al. [20], both of which modeled a sleeping state. However since the mean of the firing rates of the 80 cortical nodes was largely different from the one cortical node in the two-node model we started by finding reasonable values for the connection strengths. This was done by increasing the connection strength from thalamus to cortex until one could see a peak in the region 7.5 Hz to 15 Hz (the spindling frequency). Then increasing the connection strength from cortex to thalamus until one could see an effect on the spindles from the cortical nodes.

Then it was desired to increase the frequency of the spindles in the thalamic node as well as to get more clear SOs in the cortical node. Based on results in Caglar et al. and Jaycay et al. we chose to investigate only parameters b and μ_E to induce more down states in the cortical node and consequently more spindles in the thalamic node. Looking at the parameter searches in Figures 4.15 and 4.16 we looked for regions where there were a higher frequency of thalamic spindling while still having high values in the power spectrum of the firing rates of the cortical node. An example of that is the blue point in the figures. This point is further visualized in Figures 4.17, 4.18 and 4.19.

One can note that the firing rates of the cortical node looks very different from the

two-node model. This is expected from the results of Jaycay et al. and Cakan et al. The cortical rates in Jaycay et al. when a thalamic node is connected looks very different from Cakan et al. with only a cortical node. However slow oscillations can be seen in both cases.

5.2.2 Awake state

When trying to simulate the 81-node model in an awake state we only applied the same changes as in the two-node model. The reasoning was that the thalamic node is the same in both models and only changes in the thalamic model was made. As seen in Figure 4.20, 4.21 and 4.22 we get similar results as in the two-node model. Except that the firing rates of the cortical node look drastically different. As in the sleeping state this was expected.

6

Conclusion

A biophysically realistic thalamocortical neural mass model has been implemented. The model is a large improvement in speed compared to the previous model used by Jaycay et al. [20]. The model also simplifies further development and testing of the such a model, for example by varying the number of thalamic or cortical nodes.

Both the 2-node and 81-node model were simulated in a sleeping and an awake state. They both showed the desired behaviour. E.g. SOs in the cortical node (however not very clear in the two node model) and sleep spindles in the thalamic node in the sleeping stage while generating an alpha peak in the cortical node and no spindling in the thalamic node in the awake state.

The points found in parameter space for the different stages are not perfect. For example the alpha peaks in the awake stage have very large amplitude and are very thin which is not similar to the alpha peaks seen in experimental data. This is partly due to the complexity of quantitatively defining the desired states. Only two parameters were changed to generate the awake state, in order to get more satisfactory results it is probable that more parameters need to be varied.

Bibliography

- [1] Brain Basics: Understanding Sleep | National Institute of Neurological Disorders and Stroke, June 2022. [Online; accessed 3. Jun. 2022].
- [2] Flickr, September 2022. [Online; accessed 1. Sep. 2022].
- [3] Image of Biological Neurons connected by Synapses., September 2022. [Online; accessed 7. Sep. 2022].
- [4] thalamus | Definition, Anatomy, Function, & Disorders, September 2022. [Online; accessed 1. Sep. 2022].
- [5] L. F. Abbott. Lapicque’s introduction of the integrate-and-fire model neuron (1907). *Brain Research Bulletin*, 50:303, 1999.
- [6] Antoine R. Adamantidis, Carolina Gutierrez Herrera, and Thomas C. Gent. Oscillating circuitries in the sleeping brain. *Nat. Rev. Neurosci.*, 20:746–762, December 2019.
- [7] Anahit Babayan, Miray Erbey, Deniz Kumral, Janis Reinelt, Andrea Reiter, Josefin Röbbig, H Lina Schaare, Marie Uhlig, Alfred Anwander, Pierre-Louis Bazin, Annette Horstmann, and Arno Villringer. A mind-brain-body dataset of mri, eeg, cognition, emotion, and peripheral physiology in young and old adults. *Scientific data*, 6, February 2019.
- [8] Katarzyna Blinowska and Piotr Durka. Electroencephalography (EEG). In *Wiley Encyclopedia of Biomedical Engineering*. John Wiley & Sons, Ltd, Chichester, England, UK, April 2006.
- [9] Romain Brette and Wulfram Gerstner. Adaptive exponential integrate-and-fire model as an effective description of neuronal activity. *J Neurophysiol*, 94(5):3637–3642, July 2005.
- [10] Joana Cabral, Etienne Hugues, Olaf Sporns, and Gustavo Deco. Role of local network oscillations in resting-state functional connectivity. *Neuroimage*, 57(1):130–139, July 2011.
- [11] Caglar Cakan, Cristiana Dimulescu, Liliia Khakimova, Daniela Obst, Agnes Flöel, and Klaus Obermayer. Spatiotemporal patterns of Adaptation-Induced slow oscillations in a Whole-Brain model of Slow-Wave sleep. *Front Comput Neurosci*, 15:800101, January 2022.
- [12] Caglar Cakan, Nikola Jajcay, and Klaus Obermayer. neurolib: A Simulation Framework for Whole-Brain Neural Mass Modeling. *Cogn. Comput.*, pages 1–21, October 2021.
- [13] Caglar Cakan and Klaus Obermayer. Biophysically grounded mean-field models of neural populations under electrical stimulation. *PLOS Computational Biology*, 16(4):1–30, 04 2020.
- [14] Andrii Cherninskyi. *Human EEG with prominent alpha-rhythm*. Oct 2015.

- [15] Murat Demirtaş, Joshua B. Burt, Markus Helmer, Jie Lisa Ji, Brendan D. Adkinson, Matthew F. Glasser, David C. Van Essen, Stamatios N. Sotiropoulos, Alan Anticevic, and John D. Murray. Hierarchical Heterogeneity across Human Cortex Shapes Large-Scale Neural Dynamics. *Neuron*, 101(6):1181–119413, March 2019.
- [16] Hidenori Endo, Nobuo Hiroe, and Okito Yamashita. Evaluation of Resting Spatio-Temporal Dynamics of a Neural Mass Model Using Resting fMRI Connectivity and EEG Microstates. *Front. Comput. Neurosci.*, 0, 2020.
- [17] Wulfram Gerstner, Werner M. Kistler, Richard Naud, and Liam Paninski. *Neuronal Dynamics: From Single Neurons to Networks and Models of Cognition*. Cambridge University Press, USA, 2014.
- [18] P. Hartmann, A. Ramseier, F. Gudat, M. J. Mihatsch, and W. Polasek. [Normal weight of the brain in adults in relation to age, sex, body height and weight]. *Pathologe*, 15(3):165–170, June 1994.
- [19] A L Hodgkin and A F Huxley. A quantitative description of membrane current and its application to conduction and excitation in nerve. *J Physiol*, 117(4):500–544, August 1952.
- [20] Nikola Jajcay, Caglar Cakan, and Klaus Obermayer. Cross-frequency slow oscillation–spindle coupling in a biophysically realistic thalamocortical neural mass model. *Frontiers in Computational Neuroscience*, 16, 2021.
- [21] Khalid H. Jawabri and Sandeep Sharma. Physiology, Cerebral Cortex Functions. In *StatPearls [Internet]*. StatPearls Publishing, April 2022.
- [22] Petter Kallioinen. *EEG recording*. Mar 2012.
- [23] Giri P Krishnan, Sylvain Chauvette, Isaac Shamie, Sara Soltani, Igor Timofeev, Sydney S Cash, Eric Halgren, and Maxim Bazhenov. Cellular and neurochemical basis of sleep stages in the thalamocortical network. *Elife*, 5, November 2016.
- [24] Karine Lacourse, Jacques Delfrate, Julien Beaudry, Paul Peppard, and Simon C. Warby. A sleep spindle detection algorithm that emulates human expert spindle scoring. *Journal of Neuroscience Methods*, 316:3–11, 2019. Methods and models in sleep research: A Tribute to Vincenzo Crunelli.
- [25] L. Lapicque. Recherches quantitatives sur l’excitation électrique des nerfs traitée comme une polarisation. *Journal de Physiologie et Pathologie General*, 9:620–635, 1907.
- [26] Chris A. Mack. Analytic form for the power spectral density in one, two, and three dimensions. In *J. of Micro/Nanolithography, MEMS, and MOEMS*, 10(4), volume 10, page 040501. SPIE, October 2011.
- [27] Aakash K. Patel, Vamsi Reddy, and John F. Araujo. Physiology, Sleep Stages. In *StatPearls [Internet]*. StatPearls Publishing, April 2022.
- [28] James A. Roberts, Leonardo L. Gollo, Romesh G. Abeyesuriya, Gloria Roberts, Philip B. Mitchell, Mark W. Woolrich, and Michael Breakspear. Metastable brain waves. *Nat. Commun.*, 10, 2019.
- [29] Edmund T. Rolls, Chu-Chung Huang, Ching-Po Lin, Jianfeng Feng, and Marc Joliot. Automated anatomical labelling atlas 3. *Neuroimage*, 206:116189, February 2020.

- [30] Michael Schellenberger Costa, Arne Weigenand, Hong-Viet V. Ngo, Lisa Marshall, Jan Born, Thomas Martinetz, and Jens Christian Claussen. A thalamocortical neural mass model of the eeg during nrem sleep and its response to auditory stimulation. *PLOS Computational Biology*, 12(9):1–20, 09 2016.

A

Parameters

A.1 Model Parameters

Parameter	Value	Description	Code
C_m	$1\mu \text{ F/cm}^2$	membrane capacitance	C_m
τ_t, τ_r	20 ms	membrane time constant of TCR and TRN	tau
r_t^{max}, r_r^{max}	0.4 kHz	maximal firing rate of TCR and TRN	Q_max
θ	-58.5 mV	firing threshold (half activation)	theta
σ_t, σ_r	6 mV	inverse neural gain	sigma
γ_e	0.07 kHz	synaptic rate constant of AMPA synapses	gamma_e
γ_i	0.1 kHz	synaptic rate constant of GABA synapses	gamma_r
N_{tr}	5	connectivity constant TRN \rightarrow TCR	N_tr
N_{rt}	3	connectivity constant TCR \rightarrow TRN	N_rt
N_{rr}	25	recurrent connectivity constant in TRN	N_rr
$w_i^t = w_i^r, w_e^t = w_e^r$	1 ms	synaptic weights	g_GABA_t/r, g_AMPA_t/r?
g_t^T	3 mS/cm^2	conductance of Ca current in TCR	g_T_t
g_r^T	2.3 mS/cm^2	conductance of Ca current in TRN	g_T_r
g_h	$[0.0 - 0.08] \text{ mS/cm}^2$	conductance of rectifying current in TCR	g_h=0.062
g_{LK}	$[0.0 - 0.08] \text{ mS/cm}^2$	conductance of K leak current in TCR and TRN	g_LK_t=g_LK_r=0.032
E_{leak}	-70 mV	Nernst reversal potential for leak channels	E_L
E_e	0 mV	Nernst reversal potential of AMPA channels	E_AMPA
E_i	-70 mV	Nernst reversal potential of GABA channels	E_GABA
E_{Ca}	120 mV	Nernst reversal potential of Ca channels	E_Ca
E_K	-100 mV	Nernst reversal potential of K channels	E_K
E_h	-40 mV	Nernst reversal potential of rectifying channels	E_h
α_{Ca}	$-51.8 \cdot 10^{-6} \text{ mM/mAms}$	Ca influx rate	alpha_Ca
τ_{Ca}	10 ms	Ca time constant	tau_Ca
$[Ca_0]$	$2.4 \cdot 10^{-4} \text{ mM}$	Ca resting state concentration	Ca_0
k_1	$2.5 \cdot 10^7 \text{ kHz}$	reaction velocities of rectifying current	k1
k_2	$4.0 \cdot 10^{-4} \text{ kHz}$	reaction velocities of rectifying current	k2
k_3	$1.0 \cdot 10^{-1} \text{ kHz}$	reaction velocities of rectifying current	k3
k_4	$1.0 \cdot 10^{-3} \text{ kHz}$	reaction velocities of rectifying current	k4
n_P	4	number of Ca binding sites	n_P
g_{inc}	2.0	conductivity scaling of rectifying current	g_inc

Table A.1: thalamic parameters

A. Parameters

Parameter	Value	Description	Native
σ^{ext}	1.5mV/ms	standard deviation of external input	sigmae_ext,sigmai_ext
K_E	800	number of excitatory inputs per neuron	Ke
K_I	200	number of inhibitory inputs per neuron	Ki
$K_{E,global}$	250	number of excitatory inputs from each global area	Ke_gl
c_{EE}, c_{IE}	0.3 mV/ms	maximum AMPA PSC amplitude	cee,cie
c_{II}, c_{EI}	0.5 mV/ms	maximum GABA PSC amplitude	cii,cei
c_{global}	0.4 mV/ms	postsynaptic PSC amplitude for global connectome	c_gl
J_{EE}	2.43 mV/ms	maximum synaptic current E→E	Jee_max
J_{IE}	2.6 mV/ms	maximum synaptic current E→I	Jie_max
J_{EI}	−3.3 mV/ms	maximum synaptic current I→E	Jei_max
J_{II}	−1.64 mV/ms	maximum synaptic current I→I	Jee_max
$\tau_{s,E}$	2 ms	excitatory synaptic time constant	tau_se
$\tau_{s,I}$	5 ms	inhibitory synaptic time constant	tau_si
d_E	4 ms	synaptic delay to excitatory neurons	de
d_I	2 ms	synaptic delay to inhibitory neurons	di
τ_m	$C/g_L = 20$ ms	membrane time constant	C / gL
a	0 nS	subthreshold adaptation conductance	a
b	15 pA	spike-triggered adaptation increment	b
E_A	−80 mV	Nernst reversal potential for adaptation current	EA
τ_A	1000 ms	adaptation current time constant	tauA

Table A.2: cortical parameters

Parameter	Value	Description	Native
$N_{ctx \rightarrow thal}$	1.2	connectivity strength cortex → thalamus	Cmat[1,0]
$N_{thal \rightarrow ctx}$	0.12	connectivity strength thalamus → cortex	Cmat[0,1]
$d_{ctx \rightarrow thal}$	13 ms	synaptic thalamocortical delay	lengthMat/signalV
τ_{OU}	5 ms	time-scale of the Ornstein-Uhlenbeck process	tau_ou
σ_E	0.05 mV/ms ^{3/2}	noise variance for the cortical E population	sigma_ou
σ_I	0.05 mV/ms ^{3/2}	noise variance for the cortical I population	sigma_ou
σ_{TCR}	[0.0 − 0.005] mV/ms ^{3/2}	noise variance for the thalamic TCR population	Not present
μ_E	3.3 mV/ms	mean drift of the OU process for cortical E population	mue_ext_mean
μ_I	2.0 mV/ms	mean drift of the OU process for cortical I population	mui_ext_mean
μ_{TCR}	0mV/ms	mean drift of the OU process for thalamic TCR population	Not present
ξ	~ N(0, 1)	Gaussian white noise process	N/A
$c_{ctx-ctx}$	1	Scale factor of connection strength from cortex to cortex nodes	scale_ctx_to_ctx
$c_{ctx-thal}$	1	Scale factor of connection strength from cortex nodes to thalamus node	scale_ctx_to_thal
$c_{thal-ctx}$	1	Scale factor of connection strength from thalamus node to cortex nodes	scale_thal_to_ctx

Table A.3: Connected model parameters

A.1.1 Parameters from Cakan et al. [11]

Parameter	Value
μ_E	2.7
μ_I	3.7
b	3.2
τ_A	4765
σ_E, σ_I	0.37
C_{global}	0.3

Table A.4: Parameters from Cakan et al. for 80 node model

DEPARTMENT OF SOME SUBJECT OR TECHNOLOGY
CHALMERS UNIVERSITY OF TECHNOLOGY
Gothenburg, Sweden
www.chalmers.se



CHALMERS
UNIVERSITY OF TECHNOLOGY